frontiers | Frontiers in Remote Sensing

TYPE Original Research
PUBLISHED 29 January 2026
DOI 10.3389/frsen.2025.1692306

OPEN ACCESS

EDITED BY
Mhd. Suhyb Salama,
University of Twente, Netherlands

REVIEWED BY
Chong Shi,
Chinese Academy of Sciences (CAS), China
Thais Andrade Galvao De Medeiros,
National Institute of Space Research (INPE), Brazil

*CORRESPONDENCE
Xuerong Sun,
x.sun8@exeter.ac.uk

RECEIVED 25 August 2025
REVISED 11 December 2025
ACCEPTED 15 December 2025
PUBLISHED 29 January 2026

CITATION
Sun X, Brewin RJW, Sathyendranath S, Dall'Olmo G, Antoine D, Barlow R, Bracher A, Kheireddine M, Li M, Pitarch J, Raitsos DE, Shen F, Tilstone GH, Vellucci V and Zhang Y (2026) Coupling ecological concepts with an ocean-colour model: inversion modelling. *Front. Remote Sens.* 6:1692306. doi: 10.3389/frsen.2025.1692306

Coupling ecological concepts with an ocean-colour model: inversion modelling

Xuerong Sun[1]*, Robert J. W. Brewin[1], Shubha Sathyendranath[2,3], Giorgio Dall'Olmo[4], David Antoine[5,6], Ray Barlow[7], Astrid Bracher[8,9], Malika Kheireddine[10], Mengyu Li[11], Jaime Pitarch[11], Dionysios E. Raitsos[12], Fang Shen[13], Gavin H. Tilstone[2], Vincenzo Vellucci[6,14] and Yuan Zhang[13]

[1]Department of Earth and Environmental Sciences, Centre for Geography and Environmental Science, Faculty of Environment, Science and Economy, University of Exeter, Cornwall, United Kingdom, [2]Plymouth Marine Laboratory, Plymouth, Devon, United Kingdom, [3]Plymouth Marine Laboratory, National Centre for Earth Observation, Plymouth, Devon, United Kingdom, [4]Istituto Nazionale di Oceanografia e di Geofisica Sperimentale - OGS, Trieste, Italy, [5]Remote Sensing and Satellite Research Group, School of Earth and Planetary Sciences, Curtin University, Perth, WA, Australia, [6]Institut de la Mer de Villefranche, Sorbonne Université, National Center for Scientific Research (CNRS), Institut de la Mer de Villefranche (IMEV), Villefranche-sur-Mer, France, [7]Bayworld Centre for Research and Education, Cape Town, South Africa, [8]Phytooptics, Alfred Wegener Institute, Helmholtz Centre for Polar and Marine Research, Bremerhaven, Germany, [9]Institute of Environmental Physics, University of Bremen, Bremen, Germany, [10]Center for Remote Sensing Applications (CRSA), Mohammed VI Polytechnic University (UM6P), Ben Guérir, Morocco, [11]National Research Council (CNR), Institute of Marine Sciences (ISMAR), Rome, Italy, [12]Department of Biology, National and Kapodistrian University of Athens, Athens, Greece, [13]State Key Laboratory of Estuarine and Coastal Research, East China Normal University, Shanghai, China, [14]Sorbonne Université, CNRS, OSU Station Marines, STAMAR, Paris, France

Monitoring phytoplankton from space can help detect shifts in marine ecosystems, particularly under accelerating climate change. However, most existing ocean-colour chlorophyll-a (Chl-a) algorithms are empirical in nature, and do not explicitly consider any potential optical effects of shifts in phytoplankton community composition independent of a change in Chl-a. Similar ocean-colour signals may arise from different combinations of Chl-a and phytoplankton community composition. Revealing how phytoplankton are responding to environmental change using satellite data requires tackling this ambiguity. In previous work, we developed an Ocean Colour Modelling Framework (OCMF) to simulate ocean colour for varying Chl-a and phytoplankton size classes (PSCs). Here, we invert the OCMF to directly retrieve Chl-a, key inherent optical properties (IOPs), and PSCs, from satellite remote sensing reflectance and sea surface temperature (SST), accounting for deviations in non-algal particles (NAP) and coloured dissolved organic matter (CDOM) from assumed open ocean relationships with Chl-a. The model is validated using a global *in situ* dataset and shows stable performance across diverse oceanic conditions. Integrating ecological concepts into a bio-optical model may advance our ability to interpret long-term changes in phytoplankton community structure from space.

KEYWORDS

chlorophyll-a concentration, climate change, inherent optical properties, inversion model, ocean colour modelling framework, phytoplankton size classes, remote sensing reflectance

1 Introduction

Phytoplankton form the foundation of marine food webs and modulate planetary biogeochemical cycles, playing a key role in carbon sequestration (Longhurst et al., 1995; Field et al., 1998; Behrenfeld et al., 2006). In recent years, climate change has intensified (Terhaar et al., 2025), altering ocean temperature, stratification, and nutrient availability (Bindoff et al., 2019). Numerous studies have shown the sensitivity of phytoplankton to such environmental changes (Boyce et al., 2010; Thomas et al., 2012; Hutchins and Tagliabue, 2024; Viljoen et al., 2024), making accurate assessment of their biomass and community structure crucial for monitoring ocean ecosystems and understanding long-term changes (Sun et al., 2023, Sun et al., 2025).

Satellite ocean-colour observations are the only means of monitoring surface phytoplankton on a global scale and at high frequencies, providing synoptic and long-term data on their dynamics (McClain, 2009; Kavanaugh et al., 2021). With nearly 30 years of uninterrupted data, it is now possible to examine trends in phytoplankton at climatic scales, particularly in regions with sufficient temporal coverage (Henson et al., 2010; Hammond et al., 2020). Among the various ocean-colour products available, chlorophyll-a (Chl-a) is widely used as a proxy of phytoplankton biomass, community structure, and productivity (Platt and Sathyendranath, 2008; Sathyendranath et al., 2023). However, most standard Chl-a algorithms rely on empirical relationships (Hu et al., 2019; O'Reilly and Werdell, 2019), and do not explicitly account for influence of other optically active constituents such as non-algal particles (NAP) and coloured dissolved organic matter (CDOM). While some empirical relationships may implicitly capture changes in phytoplankton community structure (Sathyendranath et al., 2017), these assumptions may not apply across different environmental conditions (Sun et al., 2023). Other approaches, such as semi-analytical models (e.g., quasi-analytical algorithm (QAA), Garver-Siegel-Maritorena (GSM), generalized IOP (GIOP)) relate Chl-a to satellite-derived absorption and backscattering (Lee et al., 2002; Maritorena et al., 2002; Werdell et al., 2013), but they typically rely on globally tuned bio-optical parameters and rarely incorporate variability driven by phytoplankton composition or environmental factors such as sea surface temperature (SST). This can lead to ambiguity in interpretation (Defoin-Platel and Chami, 2007), since similar Chl-a concentrations can produce different ocean colours depending on the phytoplankton types present and the optical environment (Szeto et al., 2011; Alvain et al., 2012; Sauer et al., 2012), making it challenging to derive accurate phytoplankton information from ocean-colour data. Moreover, when investigating phytoplankton responses to climate change, changes in Chl-a alone can be hard to interpret, since it can vary with changes in physiology or the abundance of the cells (Siegel et al., 2013; Behrenfeld et al., 2015; Viljoen et al., 2024). A broader set of ecological and optical properties is therefore essential for understanding phytoplankton dynamics in a changing ocean (Uitz et al., 2010; Bellacicco et al., 2016; Sathyendranath et al., 2017).

With these considerations in mind, we developed the Ocean Colour Modelling Framework (OCMF), a forward ocean-colour modelling approach that simulates remote sensing reflectance (R_{rs}) based on ecological and bio-optical concepts (Sun et al., 2023; Sun et al., 2025). The OCMF explicitly accounts for size composition of phytoplankton by dividing the community into three size groups (Sieburth et al., 1978), i.e., picoplankton (<2 μm), nanoplankton (2 – 20 μm), and microplankton (>20 μm), each of which is associated with different bio-optical properties (Alvain et al., 2012; Brewin et al., 2015a; Brewin et al., 2019). The OCMF also includes the contribution of an independent background component of NAP (Stramski et al., 2001; Zhang et al., 2020). A key option within the OCMF is to incorporate SST as an independent explanatory variable, which connects phytoplankton size structure to environmental variability (Ward, 2015; Brewin et al., 2017), improving the interpretation of ocean-colour data and helping mitigate ambiguity. Through forward modelling, the OCMF enables the estimation of R_{rs} from Chl-a and SST, capturing the interactions between biological composition, optical properties, and environmental variability.

The third paper in this series focuses on the inversion of the OCMF. The goal is to retrieve multiple ecological and optical variables, including Chl-a, phytoplankton size fractions, and absorption and backscattering properties, directly from satellite-derived R_{rs} and SST. While the forward OCMF was developed for Case-1 waters (Morel and Prieur, 1977), where variations in optical properties are closely linked to Chl-a (Morel and Maritorena, 2001), the inversion framework has been extended to accommodate more optically-complex environments. To support this, two additional wavelength-independent parameters are introduced to represent deviations in NAP and CDOM contributions, similar to the Φ parameter proposed by Morel and Gentili (2009), allowing the model to account for an excess or a deficit in the inherent optical properties (IOPs) associated with these substances relative to what might be considered the norm in open ocean conditions, and retrieve them alongside Chl-a. While the OCMF inversion enables the retrieval of multiple variables, its application to large-scale or hyperspectral satellite data can be computationally demanding, due to the use of extensive parameters (Sun et al., 2025). Neural networks have been increasingly applied in ocean-colour studies due to their efficiency in handling large and complex datasets (Li et al., 2023; Zhang et al., 2024; Hammoud et al., 2025). Building on these developments, we present a neural network–based implementation of the OCMF inversion, designed to preserve ecological and optical consistency while improving computational efficiency.

Using a large dataset with global observations of Chl-a and IOPs gathered from previous studies (Sun et al., 2023; Sun et al., 2025), we conduct a comprehensive validation of the OCMF inversion model using multiple satellite datasets, including OC-CCI, GlobColour, MODIS, and Sentinel-3, as well as an independent synthetic dataset. The accuracy of the retrieval is assessed for both Chl-a and IOPs, and model sensitivity to seasonal changes is examined. We also demonstrate an application of the model using OC-CCI data for interpreting phytoplankton biomass, size structure, and optical properties from space.

2 Data

2.1 *In-situ* datasets

In total, 35,109 Chl-a measurements from the global surface ocean (≤20 m depth) were included in this study. This dataset was

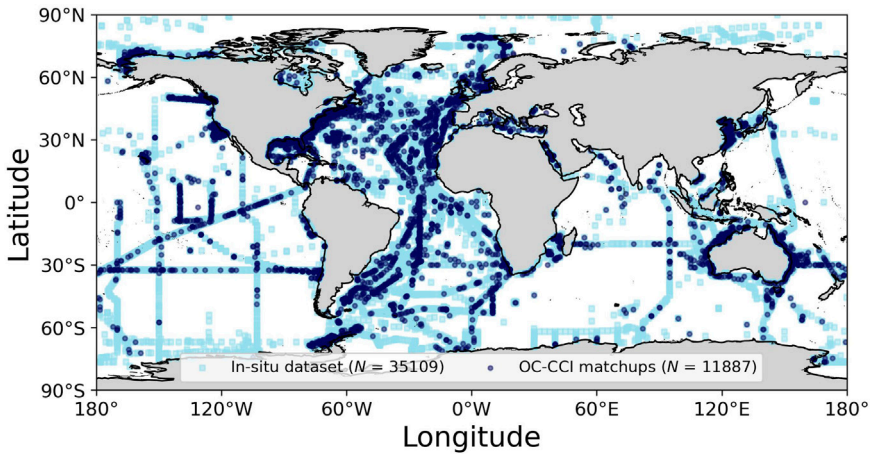

FIGURE 1
Locations of *in-situ* global Chl-a data used for validation in this study. Light blue squares represent the full dataset (N = 35,109), with dark blue dots overlaid to indicate the subset of samples matched with OC-CCI satellite data (N = 11,887). For the match-up dataset, only the shallowest sample is shown at stations with multiple depth measurements. Further details on the datasets are provided in Section 2.1, Supplementary Section S1, and in previous studies (Sun et al., 2023; Sun et al., 2025).

used to identify satellite match-ups and validate the inversion model (Figure 1). The dataset combines contributions from two earlier studies in this series of papers (Sun et al., 2023; Sun et al., 2025). These include publicly available data from multiple sources. Data portals include Australian Ocean Data Network (AODN), Biological and Chemical Oceanography Data Management Office (BCO-DMO), British Oceanographic Data Centre (BODC), Data Observation Network for Earth (DataONE), Environmental Data Initiative Data Portal (EDI), Government of Canada, NASA SeaBASS (SeaWiFS Bio-optical Archive and Storage System), and PANGAEA. Individual research programs and projects include Atlantic Meridional Transect (AMT), BOUSSOLE (Bouée pour l'acquisition de Séries Optiques à Long Terme) Project, NASA bio-Optical Marine Algorithm Dataset (NOMAD), Rothera Research Station, TARA Ocean, and Western Channel Observatory, as well as some published works. Some of these datasets were updated to include more recent measurements. Further details on the public data sources are provided in the Supplementary Section S1 and in Sun et al. (2023) and Sun et al. (2025).

The *in-situ* dataset was supplemented with additional Chl-a measurements, including those from: (1) the Atlantic Ocean (AMT cruises, Jordan et al., 2024a; Jordan et al., 2024b); (2) the Northwest Sargasso Sea [Bermuda Atlantic Time-series Study (BATS), Johnson et al., 2023]; (3) the North Pacific Ocean near Hawaii [Hawaii Ocean Time-series Data Organization and Graphical System (HOT-DOGS), HOT-DOGS, 2024]; (4) the Atlantic Southern Ocean (Viljoen and Fietz, 2021); and (5) the Chukchi Sea (Lomas, 2021).

Chl-a was measured either using the HPLC (High Performance Liquid Chromatography) method or the *in-vitro* fluorometric method. HPLC data were given the highest priority when multiple sources were available. Following earlier methodologies (Sun et al., 2023; 2025), we excluded data points where Chl-a concentrations were under 0.001 mg m^{-3} (Uitz et al., 2006) and retained only data collected from the uppermost 20 m that fall within the surface mixed layer (De Boyer Montégut et al., 2004). The dataset was split based on sampling date, using data collected before 2016 for training and after 2016 for validation to ensure independence in validation (Stock and Subramaniam, 2022), with consistent spatial coverage between the two periods (Supplementary Figure S1). Duplicate samples from different sources were removed. During validation, we retained only the shallowest sample from stations with multiple depth measurements, to best represent surface conditions.

2.2 Satellite datasets

The Ocean Colour Climate Change Initiative (OC-CCI) dataset (version 6.0, 4 km resolution, Sathyendranath et al., 2021) was used in this study (https://climate.esa.int/en/projects/ocean-colour/). For validation analyses, we used daily OC-CCI products, including optical properties at six wavelengths (412, 443, 490, 510, 560, and 665 nm) for R_{rs}, absorption of phytoplankton (a_{ph}), absorption of NAP and CDOM (a_{dg}), and backscattering of particles (b_{bp}). We also included Chl-a concentrations, estimated using a blended combination of ocean-colour algorithms (e.g., OCI, OCI2, OC2, and OCx) on merged R_{rs}, for comparison with the OCMF retrievals. In addition, water class memberships (Jackson et al., 2017) were extracted for classifying water types, ranging from open ocean to coastal waters as the class number increases. We also used an 8-day composite OC-CCI for model application (see Section 4.3). A complete list of abbreviations and symbols can be found in Supplementary Table A1 of the Appendix.

To ensure a comprehensive validation, we also included other satellite datasets to test the model inversion performance. These include: the GlobColour dataset (daily, Level 3, 4 km resolution, European Union-Copernicus Marine Service, 2022), accessed from https://data.marine.copernicus.eu/product/OCEANCOLOUR_GLO_BGC_L3_MY_009_103, which provides R_{rs} at 412, 443, 490, 555, 670 nm, along with Chl-a products derived from the sensor-specific multi-algorithm blending approach (Garnesson et al., 2019); and the

MODIS (Moderate Resolution Imaging Spectroradiometer) Aqua dataset (daily, Level 3, 4 km resolution, R2022), accessed from https://oceancolor.gsfc.nasa.gov/, which provides R_{rs} at 412, 443, 469, 488, 531, 547, 555, 645, 667, and 678 nm, as well as Chl-a products which use an ocean-colour band-ratio algorithm (OC3) and a colour index (CI) (Hu et al., 2019; O'Reilly and Werdell, 2019). Due to concerns about data quality from ageing sensors, only MODIS-Aqua data before 2020 were used in this study. The Sentinel-3 OLCI (Ocean and Land Colour Instrument) dataset (A&B, daily, Level 2, 300 m resolution, OL_L2M.003) was also used, providing R_{rs} at 400, 412, 443, 490, 510, 560, 620, 665, 673, 681 nm, along with Chl-a products which use OC4Me and CI (Morel et al., 2007). To extract match-ups between Sentinel-3 and *in-situ* measurements, we used the ThoMaS tool (https://gitlab.eumetsat.int/eumetlab/oceans/ocean-science-studies/ThoMaS), which applies spatial, temporal, and quality-control filters for accurate pixel-level extraction.

For all satellite data sources, we followed the same procedures for match-up identification and data extraction: (1) satellite data were matched with *in-situ* measurements using a spatial window of 3× 3 pixels and a daily temporal window; (2) the median of satellite-derived variables was calculated from nine pixels, and data were retained if at least five valid pixels were available; (3) for optical variables (R_{rs} and IOPs), only wavelengths within the visible range (400–700 nm) were used; (4) since the OCMF does not simulate Raman scattering, a Raman scattering correction was applied to R_{rs} before model application, following the method of Lee et al. (2013); and (5) to assess the quality of R_{rs}, QA (quality assurance) scores were calculated (Wei et al., 2016; Wei and Aurin, 2020), with wavelengths selected individually for each satellite data source.

2.3 Auxiliary datasets

2.3.1 OISST SST

The OISST (Optimal Interpolation Sea Surface Temperature, version 2, 1/4° resolution, https://psl.noaa.gov/data/gridded/data.noaa.oisst.v2.highres.html) dataset was used as the input temperature for the OCMF inversion model, which demonstrated good agreement with *in-situ* measurements (Sun et al., 2023). The daily OISST data were applied in both validation and image mapping. For validation, each *in-situ* sample was matched with OISST data based on the nearest latitude and longitude (3 x 3 pixel window in space) and daily temporal resolution. For image mapping, the spatial resolution of OISST was resampled firstly to align with the resolution of the ocean-colour satellite dataset used in the analyses, maintaining compatibility across datasets.

2.3.2 A separate dataset for validation

To evaluate the performance of the OCMF inversion model, we also used an additional independent hyperspectral synthetic dataset generated through radiative transfer simulations, as described in Pitarch and Brando (2025). This dataset provides R_{rs} at a 1-nm spectral resolution in the visible range, which serves as input for the OCMF inversion model. For our analysis, we focused on simulations with a sun zenith angle of 0°, and radiance propagation in the nadir direction (zenith angle 0°), for which azimuth is undefined and not considered, ensuring consistency with the OCMF forward model setup (Lee et al., 2011; Sun et al., 2025). Following the methodology of Pitarch and Brando (2025), SST is fixed at 20 °C for this synthetic dataset. Chl-a values in this dataset were used to evaluate the OCMF inversion model outputs.

3 Ocean colour modelling framework inversion development

The OCMF (Sun et al., 2023; Sun et al., 2025) integrates the absorption and backscattering contributions of key optically active water constituents, including phytoplankton, NAP, CDOM, and pure seawater. Variations in these constituents (except for water itself) are controlled by phytoplankton, which are divided into three size classes using a phytoplankton size structure model that accounts for their dependence on temperature (see Section 2.4 in Sun et al., 2023). When integrating the size structure model with optical models, we assumed that each size class exists in its own unique optical environment (see Section 3 in Sun et al., 2025), characterised by its own set of chlorophyll-specific IOPs. The model also includes the contribution of a background of non-algal particles. The OCMF forward modelling enables the estimation of R_{rs} from Chl-a and SST.

Here, we implement an inversion of the OCMF. This inversion allows the estimation of Chl-a and associated optical parameters directly from observed R_{rs} and SST. The following sections describe the structure, components, and implementation of the OCMF inversion modelling.

3.1 Direct OCMF inversion approach

The OCMF inversion model retrieves Chl-a using R_{rs} and SST as inputs, which can be obtained from *in-situ* measurements or satellite observations. The direct inversion employs an optimisation approach, where the forward model is used to minimise the difference between modelled and measured R_{rs} (Figure 2a).

In the forward model (Sun et al., 2025), R_{rs} is computed from total absorption ($a(\lambda)$) and total backscattering ($b_b(\lambda)$) coefficients via a semi-analytical equation that incorporates the scattering phase functions of both particles and molecules (Lee et al., 2013), such that,

$$R_{rs}(\lambda,\Omega) = \left(G_0^w(\Omega) + G_1^w(\Omega)\frac{b_{bw}(\lambda)}{\kappa(\lambda)}\right)\frac{b_{bw}(\lambda)}{\kappa(\lambda)} + \left(G_0^p(\Omega) + G_1^p(\Omega)\frac{b_{bp}(\lambda)}{\kappa(\lambda)}\right)\frac{b_{bp}(\lambda)}{\kappa(\lambda)}, \quad (1)$$

where Ω represents the sun-sensor angular geometry for R_{rs}, and $\kappa(\lambda) = b_b(\lambda) + a(\lambda)$. $G_0^w(\Omega)$, $G_1^w(\Omega)$, $G_0^p(\Omega)$, and $G_1^p(\Omega)$ are 0.0604, 0.0406, 0.0402, and 0.1310 sr^{-1}, respectively, for the observations made in the nadir direction and the sun at the zenith (Lee et al., 2011).

In Equation 1, $a(\lambda)$ is expressed as the sum of the pure water and its constituents, such that, $a(\lambda) = a_w(\lambda) + a_{ph}(\lambda) + a_d(\lambda) + a_g(\lambda)$, where $a_w(\lambda)$ is pure water absorption (Pope and Fry, 1997; Lee et al., 2015), and a_{ph}, a_d, and a_g represent phytoplankton, NAP, and CDOM absorption, respectively. Each component is represented as the sum of Chl-a for distinct size classes

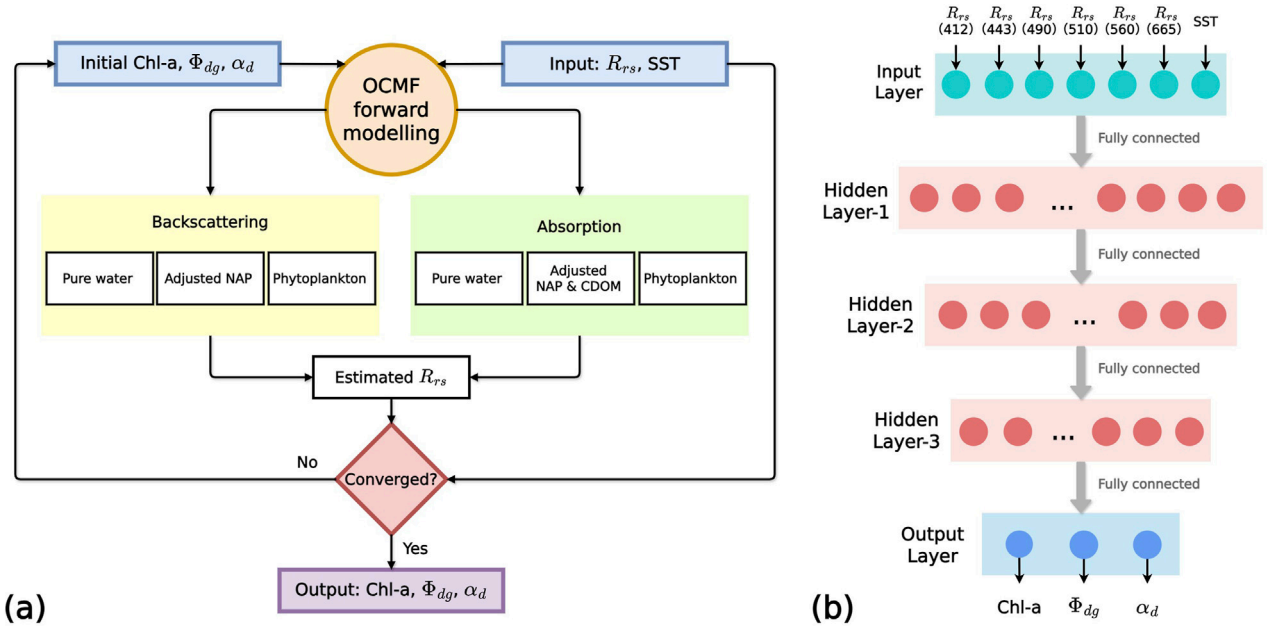

FIGURE 2
Flowchart of the OCMF inversion model, illustrating the direct inversion approach **(a)**, and the accelerated version using a neural network **(b)**. Both approaches use R_{rs} and SST as inputs, with outputs including Chl-a, Φ_{dg}, and α_d. The direct approach applies the forward OCMF model with a minimisation computation, while the accelerated approach employs a multi-layer feed forward neural network with three hidden layers with 32, 16, and 8 neurons, respectively.

(C_i, $i = 1$, 2, and 3 for pico-, nano-, and microplankton) scaled by their respective chlorophyll-specific absorption coefficients ($a^{\star}_{ph}(\lambda)$, $a^{\star}_{d,i}(\lambda)$, and $a^{\star}_{g,i}(\lambda)$), along with the background absorption coefficient of NAP ($a^{k}_{d}(\lambda)$), such that,

$$a_{ph}(\lambda) = \sum_{i=1}^{3} a^{\star}_{ph,i}(\lambda) C_i, \tag{2}$$

$$a_{d}(\lambda) = \sum_{i=1}^{3} a^{\star}_{d,i}(\lambda) C_i + a^{k}_{d}(\lambda), \tag{3}$$

and

$$a_{g}(\lambda) = \sum_{i=1}^{3} a^{\star}_{g,i}(\lambda) C_i. \tag{4}$$

Similarly, the total backscattering coefficient, $b_b(\lambda)$, consists of contributions from both pure water and particles (phytoplankton and NAP), such that, $b_b(\lambda) = b_{bw}(\lambda) + b_{bph}(\lambda) + b_{bd}(\lambda)$, where $b_{bw}(\lambda)$ is backscattering by pure water (Zhang and Hu, 2009; Zhang et al., 2009), assuming a constant salinity of 35 ppt for simplicity. Phytoplankton ($b_{bph}(\lambda)$) and NAP ($b_{bd}(\lambda)$) backscattering are represented as the sum of Chl-a in each PSC (C_i), each scaled by its corresponding chlorophyll-specific backscattering coefficient ($b^{\star}_{bph,i}$, $b^{\star}_{bd,i}$), along with the contribution of a background of NAP ($b^{k}_{bp}(\lambda)$), such that,

$$b_{bph}(\lambda) = \sum_{i=1}^{3} b^{\star}_{bph,i}(\lambda) C_i, \tag{5}$$

and

$$b_{bd}(\lambda) = \sum_{i=1}^{3} b^{\star}_{bd,i}(\lambda) C_i + b^{k}_{bp}(\lambda). \tag{6}$$

In Equations 2–6, the chlorophyll-specific absorption and backscattering coefficients of different water constituents are adopted from Sun et al. (2025). The primary unknown is the total Chl-a, but it is represented here as the sum of the three size-fractionated components (C_i), through incorporating the SST-dependent three-component model (Sun et al., 2023), where the other input, SST, is introduced to determine the proportions of total Chl-a attributed to the three size classes.

The forward model (Sun et al., 2025) follows the classical Case-1 water assumption, which may limit its applicability in optically complex waters (e.g., coastal regions). To address this, the inversion model introduces two wavelength-independent parameters, Φ_{dg} and α_d, which capture deviations from the Case-1 assumption, representing excesses or deficits of $a_d(\lambda)$, $a_g(\lambda)$, and $b_{bd}(\lambda)$ relative to their assumed values of one, similar to the Φ parameter proposed by Morel and Gentili (2009). For example, in coastal or high-CDOM environments, they may deviate from 1, reflecting variations in optical properties from standard global, open-ocean conditions. Given the similar spectral shapes of $a_d(\lambda)$ and $a_g(\lambda)$, distinguishing between these two components using multispectral data is challenging. Therefore, Φ is explicitly defined with reference to $a_{dg}(\lambda)$, and Equations 3, 4 are rewritten as,

$$a_{dg}(\lambda) = \left\{ \sum_{i=1}^{3} a^{\star}_{d,i}(\lambda) C_i + a^{k}_{d}(\lambda) + \sum_{i=1}^{3} a^{\star}_{g,i}(\lambda) C_i \right\} \Phi_{dg}. \tag{7}$$

Similarly, α_d is a wavelength-independent factor that accounts for variations in b_{bd}, in a similar manner to Φ_{dg} for a_{dg}. Therefore, Equation 6 is rewritten as,

$$b_{bd}(\lambda) = \left\{ \sum_{i=1}^{3} b^{*}_{bd,i}(\lambda) C_i + b^{k}_{bp}(\lambda) \right\} \alpha_d. \quad (8)$$

By introducing Φ_{dg} and α_d in Equations 7, 8, the inversion model is taken forward to estimate three unknowns, Chl-a, Φ_{dg}, and α_d (Figure 2a). These variables are retrieved by minimising the difference between observed and modelled R_{rs} using a minimisation method ('lmfit' package in Python).

Two SST-dependent phytoplankton size structure models (16- and 17-parameter approaches, Sun et al., 2023) are available to derive size-fractionated Chl-a for each pair of total Chl-a and SST, resulting in two corresponding sets of bio-optical parameters (Sun et al., 2025). To streamline the presentation and avoid redundancy, results from the 16-parameter model are shown in the main text, and those of the 17-parameter model in the Supplementary.

3.2 Accelerated OCMF inversion using neural network

The OCMF inversion model (Section 3.1) involves a large set of parameters (i.e., those in phytoplankton size structure model, size-fractionated chlorophyll-specific absorption and backscattering coefficients), which increases computational cost, especially for satellite applications. To address this, we implemented an acceleration method that replaces the minimisation process with a neural network-based trained model that is able to estimate results rapidly.

A multi-layer feed forward neural network (NN) was developed to retrieve Chl-a, Φ_{dg}, and α_d, by learning their relationships with R_{rs} and SST. To train the NN, a large OCMF synthetic dataset was first generated to reflect realistic global-ocean conditions, with Chl-a, SST, Φ_{dg}, and α_d as inputs. These inputs were introduced into the OCMF forward model (Sun et al., 2025) to compute the corresponding R_{rs} as output, forming a lookup table for NN training. During sampling, Chl-a was sampled randomly from a log-normal distribution spanning 0.001 to 100 mg m^{-3}, ensuring coverage of diverse oceanic conditions. SST values were uniformly sampled between −1.8 and 40 °C, capturing conditions from polar to tropical waters. Parameters Φ_{dg} and α_d followed log-normal distributions, with values ranging from 0.001 to 12, a deliberately broad range that covers values derived from *in-situ* measurements and calculations. A total of 200 logarithmically (Chl-a, Φ_{dg}, α_d) or linearly (SST) spaced values were generated for each variable. Weighted random sampling was applied to Chl-a, Φ_{dg}, and α_d, based on their probability distributions to better reflect their natural variability. Additionally, to generate a comprehensive dataset efficiently, 100 blocks of 4 million samples each were created and stored for further training processes.

The NN consists of four fully connected layers (Figure 2b), with an input layer of seven features: R_{rs} at the OC-CCI wavelengths (412, 443, 490, 510, 560, 665 nm) and SST, obtained from the OCMF synthetic dataset. Three hidden layers with 32, 16, and 8 neurons, respectively, use the ReLU (rectified linear unit) activation function (Kingma and Ba, 2014), while the output layer contains Chl-a, Φ_{dg}, and α_d, corresponding to the input from the OCMF synthetic dataset. The input and output data were log-transformed and standardised before training. The model was trained using the Adam (adaptive moment estimation) optimizer (learning rate = 0.001, batch size = 10,240) for up to 12,000 epochs, with early stopping (patience = 1,000 epochs) to prevent overfitting (Prechelt, 1998; Nair and Hinton, 2010). During training, the synthetic dataset was randomly split into 80% for training and 20% for internal validation, and processed in batches. Each dataset block (N = 100) was processed separately, and the corresponding trained models and specific scalers were stored individually for further application. During internal validation, all 100 models achieved a coefficient of determination greater than 0.99 and a root mean squared difference below 0.04 for Chl-a in $\log_{10}$ space.

Once trained, the NN was applied to R_{rs} and SST using the 100 trained models. The input data were standardised with the corresponding scalers, converted to PyTorch tensors, and processed with GPU acceleration to retrieve scaled Chl-a, Φ_{dg}, and α_d, which were then inverse-transformed to their original units. The final retrievals across all blocks were aggregated, with the median computed and stored for further analysis. This accelerated approach, referred to as OCMF-NN, significantly reduces computational cost compared to the direct OCMF inversion method. For example, on a dataset of 20,000 samples, the direct OCMF inversion takes approximately 2,500 s, whereas the OCMF-NN approach reduces this to 30 s, enabling large-scale applications for global climate studies. In this study, the OCMF-NN was trained with OC-CCI wavelengths; however, it can be applied to other satellite sensors by retraining the model with R_{rs} inputs for the corresponding sensor-specific wavebands.

3.3 Statistical tests

Model performance was evaluated using several statistical metrics, including the Pearson correlation coefficient (r), significance level (p), bias (δ), mean absolute difference (MAD, ϵ), root mean squared difference (RMSD, ψ), centre-pattern root mean square difference (Δ), and regression slope (S), based on comparison between observed and estimated values. The δ, ϵ, ψ, and Δ were calculated following previous studies (Brewin et al., 2015b; Sun et al., 2023; Sun et al., 2025). The slope (S) and intercept (I) were determined through linear least-squares regression between estimated and measured values, $X_i^E = SX_i^M + I$, where X is the variable of interest (e.g., Chl-a concentration, IOPs), E and M refer to estimated and measured variables, respectively. Given the log-normal distribution of bio-optical properties in the ocean (Campbell, 1995), statistical analysis for Chl-a and IOPs were calculated in $\log_{10}$ space.

4 Results and discussion

4.1 Model validation

4.1.1 OC-CCI dataset

The OCMF was developed to retrieve Chl-a, PSCs and IOPs within a consistent framework that, unlike purely empirical

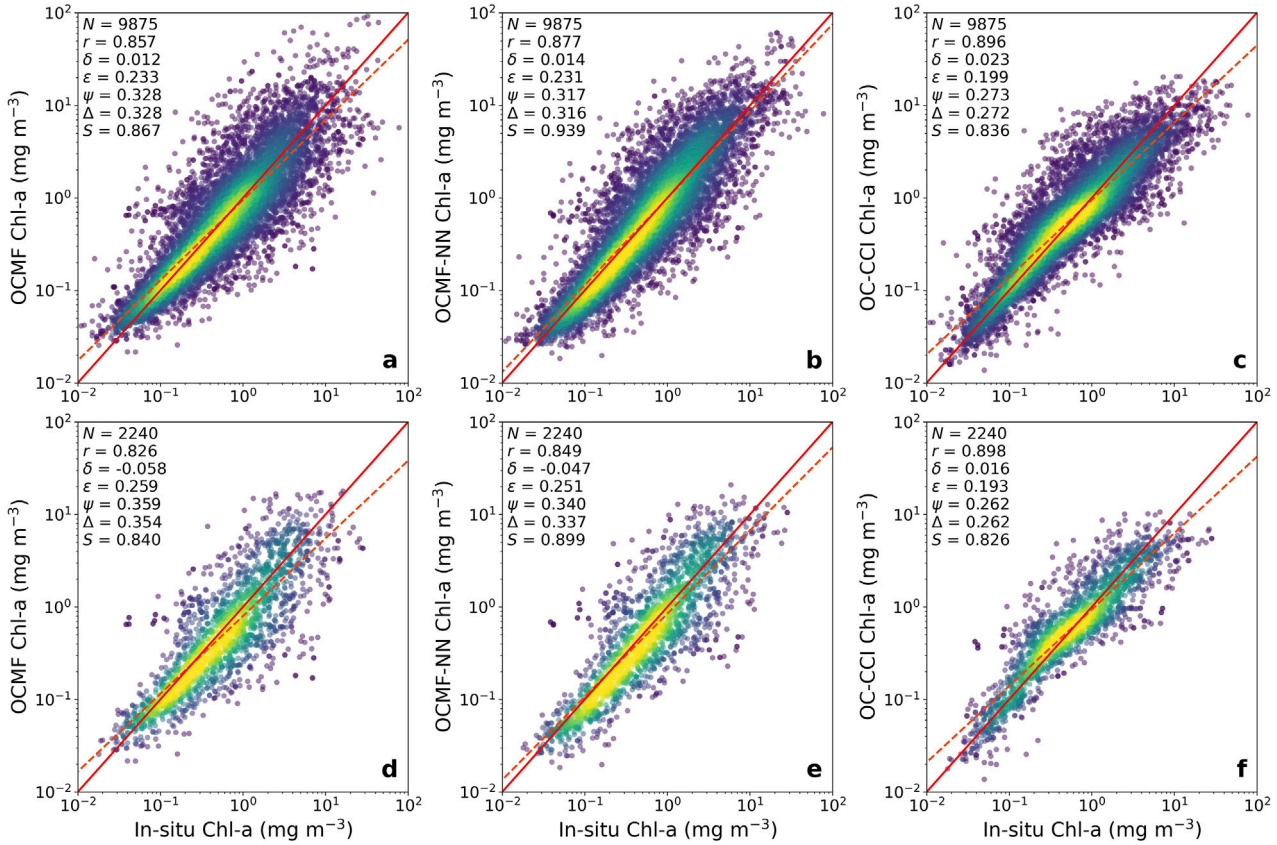

FIGURE 3
Validation of Chl-a estimates (y-axis) against *in-situ* observations (x-axis), using the full dataset **(a–c)** and an independent validation dataset collected after 2016 **(d–f)**. Results are based on the application of the OCMF inversion using daily OC-CCI and OISST products. Panels show results from the OCMF direct inversion (left column), the OCMF-NN approach (middle column), and the standard OC-CCI Chl-a product (right column). The solid red line indicates the 1:1 line, while the dashed line shows the linear least-squares regression fit in $\log_{10}$ space. The model is based on the 16-parameter model (Sun et al., 2023). Results using the 17-parameter model are shown in Supplementary Figure S2.

algorithms, aligns with the characteristics needed for interpreting ocean-colour for climate-change studies (Sathyendranath et al., 2017). However, empirical algorithms are known to set the standard in performance when evaluated with discrete match-ups (Brewin et al., 2015b), and have consequently been adopted by space agencies when generating standard products of Chl-a. Therefore, a key step in evaluating our inversion of the OCMF is to compare performance in Chl-a retrievals with the empirical algorithms considered to be the gold standards, using a discrete match-up dataset.

Using the OC-CCI dataset, we present a global validation of Chl-a retrievals derived from OCMF, OCMF-NN, and compare them with the OC-CCI standard products (Figure 3). OCMF and OCMF-NN retrievals were obtained by applying the inversion model (direct or accelerated with NN) to the matched OC-CCI R_{rs} and OISST SST. To ensure data quality, R_{rs} measurements with a QA score below 0.8 were removed, and only the shallowest depth measurements were used when multiple depths were available. Retrievals with extreme Φ_{dg} and α_d values were excluded (e.g., outside the range 0.1–10.0), retaining over 97.5% of the data. To avoid redundancy, results shown here are from the 16-parameter model, with the 17-parameter results available in the Supplementary. The two models show broadly comparable results at the global scale.

The OCMF inversion model shows a strong correlation with *in-situ* Chl-a, with r = 0.857 for the full dataset and 0.826 for the independent dataset (Figures 3a,d). The OCMF-NN has similar performance (r = 0.877 and 0.849), demonstrating that the NN preserves the performance of the direct inversion model (Figures 3b,e). The OC-CCI standard products have slightly higher correlation (r = 0.896 and 0.898) and lower RMSD (ψ = 0.273 and 0.262), particularly in the independent dataset (Figures 3c,f). However, compared to OC-CCI, OCMF exhibits a lower bias and a regression slope closer to one, especially for the full dataset (δ = 0.012, S = 0.867).

To evaluate further the OCMF and OCMF-NN models under varying environmental conditions, we assessed Chl-a retrieval performance across different Chl-a ranges (Figure 4), time periods, oceanic regions, and water classes (see Supplementary Section S4.1), using the same OC-CCI validation dataset. A key advantage of OCMF and OCMF-NN is their ability to provide consistent Chl-a estimates across both spatial and temporal scales (Figure 4; Supplementary Figure S8). Figure 4 shows the relative residuals between estimated and measured values ($X_i^E/X_i^M - 1$) for four Chl-a ranges (<0.1, 0.1–1, 1–10, and >10 mg m^{-3}). Medians and standard deviations of the residuals within each range are reported, where positive values indicate overestimation and

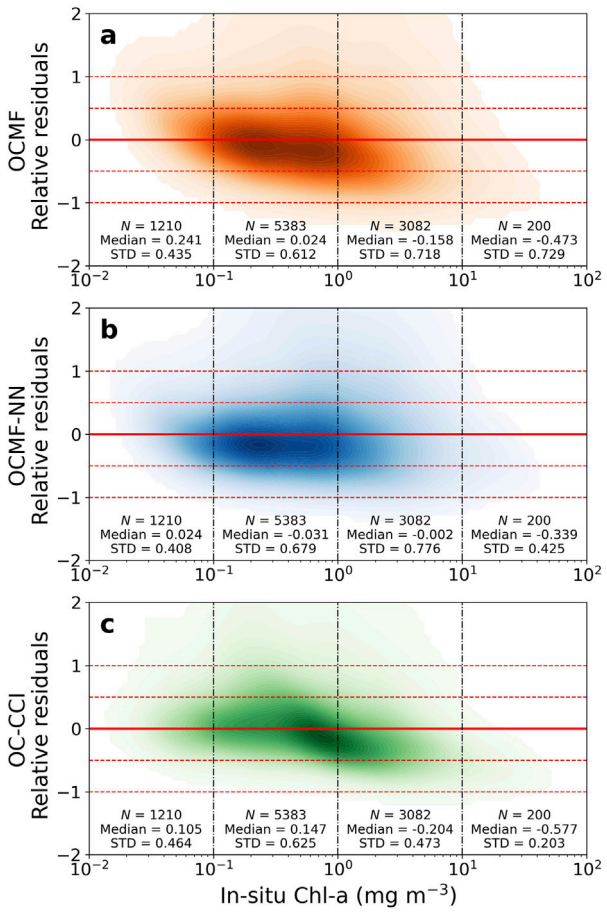

FIGURE 4
Relative residuals of Chl-a retrievals (y-axis) from the OCMF **(a)**, the OCMF-NN **(b)**, and OC-CCI **(c)**, compared against *in-situ* Chl-a measurements across four concentration ranges (<0.1, 0.1–1, 1–10, and >10 mg m^{-3}), with median and standard deviation provided, based on the full validation dataset. The solid line represents zero residual, while dashed lines indicate residuals of ±0.5 and ±1.0. The model is based on the 16-parameter model (Sun et al., 2023). Colour intensity corresponds to data density. Results using the 17-parameter model are shown in Supplementary Figure S3.

negative values indicate underestimation. OC-CCI systematically overestimates Chl-a at low concentrations (median relative residual = 0.105 and 0.147 for <0.1 mg m^{-3} and 0.1–1 mg m^{-3}, respectively) and underestimates at higher concentrations (−0.204 and −0.577 for 1–10 mg m^{-3} and >10 mg m^{-3}, respectively; Figure 4c), likely due to regional dependencies of the applied empirical algorithms (Sathyendranath et al., 2001; Brewin et al., 2015a; Lavigne et al., 2021; Dierssen and Smith, 2000). In contrast, both OCMF and OCMF-NN improve performance by reducing bias across a range of trophic regimes, providing more consistent estimates (Figures 4a,b), which is crucial for global studies requiring reliable Chl-a retrievals in diverse environments. Similarly, OCMF and OCMF-NN maintain a stable regression slope close to 1 across years (Supplementary Figure S8), whereas OC-CCI shows fluctuations in slope, indicating that the OCMF may provide a more stable representation of long-term changes, which is important for applications such as climate studies and trend analysis (Sathyendranath et al., 2017; Pauthenet et al., 2024).

However, regional and optical environment assessments reveal specific limitations of the OCMF inversion model (Supplementary Figures S10, S12). While all models perform well in the Atlantic, Pacific, and Indian Oceans, their accuracy decreases in polar regions (Supplementary Figure S10), likely due to under-representation of *in-situ* dataset during model development and the distinct optical properties of these waters (Babin et al., 2015). For example, in the Arctic, high CDOM and NAP absorption can lead to the overestimation of Chl-a (e.g., Lewis and Arrigo, 2020; Li J. et al., 2024), whereas in the Antarctica, differences in phytoplankton community structure and the optical properties of both phytoplankton and non-algal constituents introduce additional uncertainty (e.g., Robinson et al., 2021; Salyuk et al., 2025). In coastal waters, lower Chl-a accuracy may result from reduced reliability in satellite R_{rs}, as atmospheric correction is more challenging due to adjacency effects from land and variable aerosol conditions (e.g., Bulgarelli and Zibordi, 2018). Across different optical environments, OC-CCI shows slightly better performance in clear open-ocean waters, but all models exhibit higher uncertainties in optically complex regions (Supplementary Figure S12), consistent with previous studies (Jackson et al., 2017; Sathyendranath et al., 2019). This underlines the persistent difficulty of retrieving Chl-a in waters with NAP and CDOM that varies independently of Chl-a (Blondeau-Patissier et al., 2014).

In all assessments mentioned above, OCMF-NN achieves accuracy comparable to OCMF, despite relying on a simple machine learning approach without extensive parameter tuning. Its lightweight neural network architecture balances computational efficiency with reduced risk of overfitting. While more complex artificial intelligence models may improve accuracy (Pahlevan et al., 2022; Zhang Y. et al., 2023), our approach prioritises simplicity and strict alignment with the conceptual framework of the OCMF. The reliability of OCMF-NN stems from the theoretical rigour of the OCMF forward model, which ensures the training lookup table captures realistic optical variability.

The validation of IOPs (i.e., a_{ph}, a_{dg}, and b_{bp}) between measured and OCMF-derived values further demonstrates the capability of the model (see Supplementary Section S4.2.1). While the OC-CCI standard IOP products generally show slightly lower RMSD and higher correlations, OCMF has comparable results and outperforms the OC-CCI in some cases (Supplementary Figures S14, S16, S18). In general, OCMF provides improved estimates of a_{ph}, comparable performance for b_{bp}, and shows slightly increased variability in the retrieval of a_{dg}. A key limitation of standard ocean-colour products is their reliance on separate algorithms for retrieving different variables, each based on distinct assumptions about water constituents and optical properties. For example, Chl-a is retrieved using OCx or CI algorithms (O'Reilly and Werdell, 2019; Hu et al., 2019), whereas IOPs are estimated using models such as QAA (Lee et al., 2002). This can lead to inconsistencies when combining outputs, as each algorithm has its own error characteristics (Brewin et al., 2015b; Zheng and DiGiacomo, 2017), potentially affecting further applications, for example, in biogeochemical modelling (Ciavatta et al., 2018; Ciavatta et al., 2019; Pradhan et al., 2020). Besides, the use of multiple algorithms requires users to be familiar with the parameter settings and limitations of each model.

In contrast, OCMF retrieves Chl-a and all key optical properties simultaneously within a single inversion framework, ensuring greater internal consistency and simplifying integration for applications. More importantly, OCMF explicitly incorporates chlorophyll-specific bio-optical properties and accounts for their variations with phytoplankton size structure and temperature, different from standard algorithms that often assume fixed relationships, limiting their reliability across spatial and temporal scales (Brown et al., 2008; Brewin et al., 2015a; Lee et al., 2020). This enables OCMF to address ambiguity in interpreting ocean colour related to differing combinations of phytoplankton sizes and Chl-a concentrations.

4.1.2 Other datasets

Beyond OC-CCI, validation of the OCMF inversion model using multiple satellite products demonstrates its broad applicability (see Supplementary Section S4.2.2; Supplementary Table S1). Comparisons with GlobColour, MODIS, and Sentinel-3 show that while standard products often achieve slightly better performance (e.g., higher correlation coefficient, lower bias) in estimating Chl-a, OCMF offers stable and consistent performance across different datasets.

In general, GlobColour standard Chl-a products perform well (Supplementary Figure S20), as Chl-a is estimated separately for each sensor using its specific R_{rs}, accounting for sensor-specific spectral and spatial characteristics (Garnesson et al., 2019). This also supports good performance for single-sensor datasets such as MODIS and Sentinel-3 (Supplementary Figures S21, S22), which rely on empirical algorithms (e.g., OCx and CI) optimised using large *in-situ* datasets and calibrated for each sensor (O'Reilly and Werdell, 2019). In contrast, OCMF uses absolute R_{rs} values, making its performance highly sensitive to the quality of those inputs. For example, the slightly lower accuracy of OCMF-derived Chl-a from MODIS data, compared to the standard product, may result from the use of all visible wavebands of MODIS, some of which are known to be biased or less suitable for ocean-colour retrievals (Mélin et al., 2007; Hu et al., 2012; Bisson et al., 2021). This highlights the requirement of strict quality control of the input R_{rs} when applying OCMF to specific sensors, particularly for those with known degradation or spectral limitations. Additionally, non-ocean-colour satellite missions may offer complementary water-optical information and could be evaluated as supplementary data sources in future applications (Shi et al., 2021; Zhang X. et al., 2023).

Beyond satellite validation, good agreement was also observed between simulated and retrieved Chl-a using the synthetic dataset from Pitarch and Brando (2025), further supporting the reliability of the OCMF inversion model (see Supplementary Section S4.2.3). The Chl-a retrieval accuracy was higher than that in the satellite validation, likely due to the controlled optical conditions in the synthetic dataset (Supplementary Figure S23). Results also suggest that retrievals from hyperspectral (1-nm) data have slightly higher accuracy than those from multispectral (OLCI bands) retrievals (not shown). This aligns with previous studies that highlight the advantages of hyperspectral data for ocean-colour applications (Bracher et al., 2020; Dierssen et al., 2023), and demonstrates that OCMF can be easily applied to hyperspectral satellite observations (e.g., NASA PACE [Plankton, Aerosol, Cloud, ocean Ecosystem]), with the potential for improved performance.

4.2 Model sensitivity to seasonal changes: a case study at BOUSSOLE

We evaluated the sensitivity of the OCMF inversion model to seasonal changes using a long time series from the BOUSSOLE Project in Western Mediterranean Sea. By applying OCMF to OC-CCI daily R_{rs} products, we generated biweekly Chl-a climatologies and compared them with *in-situ* measurements (BOUSSOLE Project monthly cruise) and the OC-CCI standard Chl-a products (Figure 5a).

The *in-situ* Chl-a measurements exhibit clear seasonal patterns, characterised by a spring bloom between March and April (biweeks 6–8), followed by a post-bloom decline, low Chl-a concentrations throughout summer and autumn (biweeks 11–22), and a winter increase. Seasonal changes in physical and biogeochemical conditions are responsible for the observed variation in Chl-a (i.e., mixed layer depth dynamics, Marty et al., 2002; Volpe et al., 2012). Both satellite-derived Chl-a (OCMF and OC-CCI) capture these seasonal patterns but differ in their accuracy. A linear regression analysis between SST and $\log_{10}$-transformed Chl-a using the biweekly climatology dataset (N = 25, excluding the first and last biweeks due to a lack of *in-situ* data) showed that *in-situ* Chl-a decreases significantly with SST (slope = −0.0769, $p < 0.01$). The OCMF-derived Chl-a (slope = −0.0505) exhibited a similar negative relationship, with the slope aligning more closely with the *in-situ* trend than that of the OC-CCI product (slope = −0.0361), though both slopes were statistically significant ($p < 0.01$). This result suggests that OCMF has a slightly better representation of the seasonal variability in Chl-a at BOUSSOLE.

During winter and spring, both satellite products tend to underestimate Chl-a, with OCMF showing slightly lower values than OC-CCI. In summer and autumn, OC-CCI overestimates Chl-a significantly, especially at low concentrations, reflecting known biases in standard algorithms in this region (Bricaud et al., 2002; Volpe et al., 2007; Kournopoulou et al., 2024). OCMF, however, shows better agreement with *in-situ* measurements, particularly in capturing the lower values during these seasons. Although BOUSSOLE surface waters are classified as Case-1 water (Antoine et al., 2008), seasonal variations in α_d parameter through OCMF inversion suggest that NAP backscattering (b_{bd}) does not follow a fixed covariation with Chl-a (Figure 5b), as assumed in standard Case-1 models. For example, during the bloom, α_d reaches its lowest value (around 0.5), as phytoplankton dominate backscattering, reducing the relative contribution of NAP. Following the bloom, α_d rises sharply over one, likely due to increased detrital material from grazing and cell degradation. In summer and autumn, α_d remains high, which could result from the fragmented detritus from smaller phytoplankton. In winter, α_d drops, possibly due to the dilution of particles in the mixed layer. This pattern aligns with previous observations that the ratio of b_{bp} and Chl-a is higher than expected in certain seasons, and its variability follows a strong seasonal cycle in this region (Antoine et al., 2011; Loisel et al., 2011). For the Φ_{dg} parameter, its relative stability throughout the year is consistent with previous observations that a_{dg} follows a similar seasonal pattern to Chl-a (Organelli et al., 2016; Álvarez et al., 2023). However, given that the region is thought to have systematically higher CDOM per unit Chl-a compared to standard Case-1 water, particularly in summers

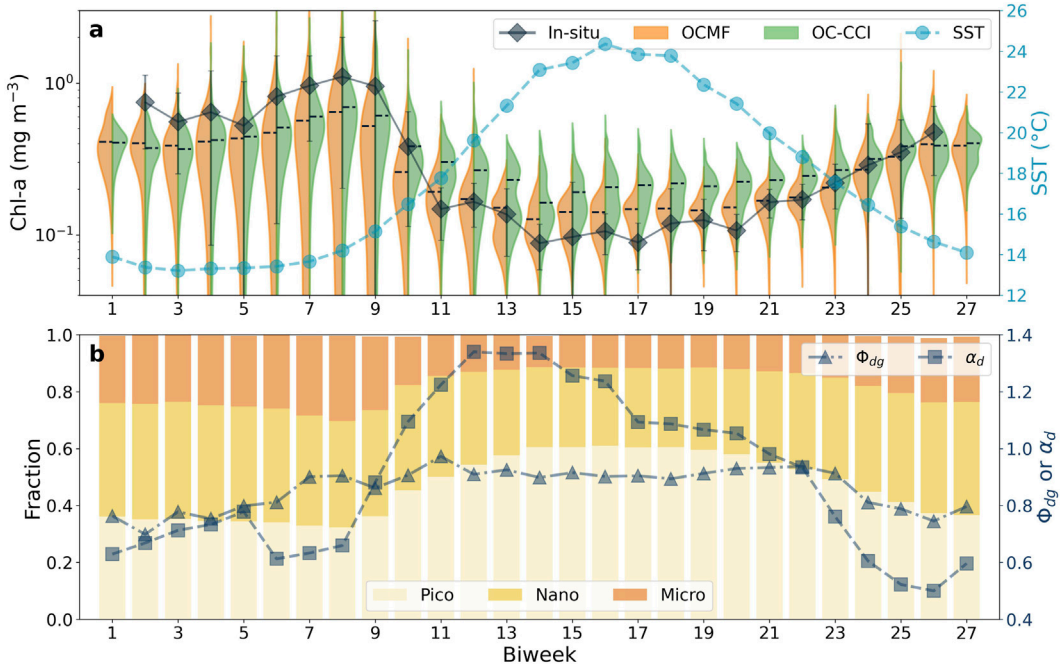

FIGURE 5
Sensitivity of the OCMF inversion model to seasonal changes at the BOUSSOLE site, using OC-CCI (R_{rs} and Chl-a) and OISST daily products between 1997 and 2024. Biweekly climatologies of Chl-a derived from the OCMF direct inversion (orange, left side of each violin plot) and the OC-CCI product (green, right side) are shown, with dashed lines inside indicating median values. *In-situ* Chl-a measurements are overlaid with black lines. Seasonal variations in SST are shown as blue dashed line on the right y-axis **(a)**. Biweekly variations in phytoplankton size composition from the OCMF inversion are presented as stacked bars, showing the percentage of pico-, nano-, and microplankton. Overlaid are the seasonal patterns of Φ_{dg} (triangles) and α_d (squares) plotted on right the y-axis **(b)**. The model is based on the 16-parameter model (Sun et al., 2023). Results using the 17-parameter model are shown in Supplementary Figure S4.

(Organelli et al., 2014), a higher Φ_{dg} derived from the inversion model would be expected. Instead, the model returns a Φ_{dg} value below one, suggesting that the a_{dg} maybe underestimated (seen in a_g validation, not shown). This could explain the slight overestimation of Chl-a during summer, as the model may attribute more of the total absorption to phytoplankton.

Seasonal shifts in phytoplankton community structure is evident in OCMF-derived PSCs (Figure 5b), which are consistent with trends observed in HPLC-derived *in-situ* measurements (not shown). In winter and early spring, the violin plots (Figure 5a) show narrow peaks, suggesting a more consistent Chl-a concentrations inter-annually. Together with the PSCs, this suggests a relatively uniform phytoplankton community dominated by nano- and picoplankton. These patterns are likely driven by deep winter mixing and sufficient nutrient availability, which create uniform environmental conditions (Lavigne et al., 2013). Starting in spring, the Chl-a range becomes wider, indicating variability in phytoplankton growth intensity (Kheireddine and Antoine, 2014; Mayot et al., 2017). During this period, microplankton, such as diatoms, increase and contribute to the increased Chl-a concentrations. From late spring onward, the Chl-a concentration becomes more variable, as indicated by the broad range and dual peaks in the violin plots, potentially influenced by shifts in community structure, due to distinct responses of different phytoplankton classes to environmental conditions. PSCs derived from OCMF show that small phytoplankton (nano- and picoplankton) dominate throughout the year, with picoplankton peaking in summer (Figure 5b). This pattern is consistent with previous studies, where *Synechococcus* and *Prochlorococcus* thrive in summer under stratified, low-nutrient conditions (Navarro et al., 2017; El Hourany et al., 2019).

At BOUSSOLE, the OCMF seems to capture seasonal variations, offering an improved representation of bio-optical dynamics by accounting for the influence of non-algal substances and improving Chl-a estimations relative to standard products. Additionally, OCMF provides information on PSCs, further enhancing its utility for biogeochemical studies. However, some discrepancies remain, such as potential biases in the Φ_{dg} parameter. It should be acknowledged that the OCMF was trained on a broad global dataset and was not specifically tailored for this region.

4.3 Model applications

We applied the OCMF-NN inversion model to the Southern Ocean, Atlantic section, using R_{rs} and SST from an 8-day composite OC-CCI product (17th to 24th January 2004) and a corresponding 8-day averaged OISST product, respectively. This region was selected because it represents an optically complex environment, spanning coastal and oceanic waters with diverse ecological and optical characteristics, with a wide range of temperature variations (i.e., −1.8–26 °C), and concurrent *in-situ* measurements are available for validation. Figure 6 shows the spatial distribution of model-derived Chl-a, Φ_{dg}, α_d, fraction of microplankton to Chl-a (F_3),

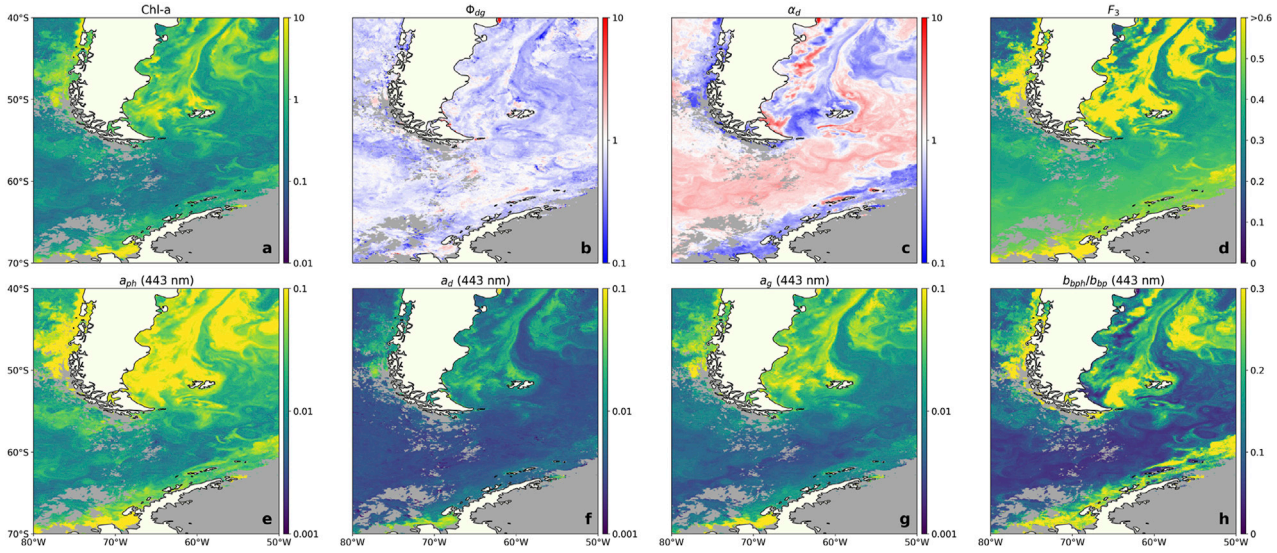

FIGURE 6
Satellite-derived estimates over the Atlantic sector of the Southern Ocean, based on the OCMF-NN inversion model applied to an 8-day composite (17–24 January 2004) of OC-CCI (R_{rs}) and OISST products, including Chl-a **(a)**, Φ_{dg} **(b)**, and α_d **(c)**. Additional variables retrieved from the inversion include the fraction of microplankton **(d)**, and absorption coefficients at 443 nm for phytoplankton **(e)**, NAP **(f)**, and CDOM **(g)**, along with the ratio of particulate backscattering at 443 nm attributed to phytoplankton relative to the total particles **(h)**. The model is based on the 16-parameter model (Sun et al., 2023). Results using the 17-parameter model are shown in Supplementary Figure S5.

absorption properties (a_{ph}, a_d, a_g), and backscattering properties (ratio of b_{bph} and b_{bp}).

The OCMF-NN-derived Chl-a in January exhibits distinct latitudinal variations. On the Patagonian Shelf, microplankton dominates in areas with high Chl-a, consistent with previous studies showing that diatoms and dinoflagellates are the primary phytoplankton groups during bloom events (Garcia et al., 2008; Guinder et al., 2024). Some coastal patches exhibit a slightly higher fraction of nanoplankton (Supplementary Figure S6), which could be associated with the presence of coccolithophores during the season (Signorini et al., 2006). Without concurrent *in-situ* phytoplankton data, it is challenging to determine the exact community composition. However, bio-optical parameters such as α_d and the ratio of b_{bph} and b_{bp} maps may provide insights into the types of phytoplankton present (Figures 6c,h). For example, areas dominated by coccolithophores are expected to show higher α_d and lower b_{bph} and b_{bp} ratios, due to enhanced backscattering from inorganic particles (Balch et al., 2014).

Chl-a concentration decreases towards the Drake Passage, reaching low values around the Antarctic Polar Front region, before increasing again near the Antarctic shelf. This pattern is consistent with previous observations (Demidov et al., 2010). Across the Drake Passage, nanoplankton dominate the phytoplankton community (40%–50%), such as haptophytes (coccolithophores), which are characterised by higher α_d values and lower b_{bph} and b_{bp} ratios. Microplankton also contribute significantly, with a clear gradient of increasing fraction toward the south (Figure 6d). This shift is probably associated with the Antarctic Polar Front, which acts as a biological boundary, with diatoms being more dominant in the colder and silicate-rich Antarctic waters (Hayward et al., 2024).

Previous studies of Chl-a distribution and phytoplankton communities in the western Antarctic Peninsula region during summer (Trimborn et al., 2015; Arrigo et al., 2017; Schofield et al., 2017; Biggs et al., 2019) are generally consistent with the results of this study. Coastal and shelf waters of the Antarctic Peninsula (e.g., Marguerite Bay) are known to exhibit phytoplankton blooms with high Chl-a concentrations, where large phytoplankton (e.g., diatoms) are dominant. In contrast, in the continental shelf and open waters, the contribution of microplankton generally decreases, but often remains significant, while nanoplankton (e.g., cryptophytes) also play an important role, with local variability in the region. This spatial distribution could be affected by sea-ice melt, which influences nutrient availability and water-column stratification (Ferreira et al., 2024).

The general pattern of OCMF-NN-derived Chl-a is consistent with the OC-CCI standard product, though the OCMF-NN model retrieves higher Chl-a values across most regions (Supplementary Figure S7). Previous studies found that standard Chl-a algorithms tend to overestimate low Chl-a concentrations and underestimate high concentrations in this region (e.g., Argentine Patagonian Shelf, Southern Ocean, Dogliotti et al., 2008; Johnson et al., 2013). A small amount of concurrent *in-situ* match-ups from the Antarctic Peninsula, collected during the period of the 8-day composite (N = 13), are overlaid on the satellite image (Supplementary Figure S7), showing that the OC-CCI standard product tends to underestimate Chl-a (bias = −0.349), whereas OCMF-NN shows much lower bias (0.040). This discrepancy is often linked to regional variations in bio-optical properties. For example, in the Southern Ocean, lower Chl-a-specific absorption results from a higher proportion of microplankton per unit Chl-a, combined with distinct CDOM absorption and particulate backscattering, contributing to an overall underestimation in Chl-a retrievals by global empirical algorithms (Ortega-Retuerta et al., 2010; Ferreira et al., 2018; Robinson et al., 2021). These bio-optical characteristics

align with the predominance of large-celled phytoplankton in cold oceanic regions (Marañón et al., 2012; Ward, 2015). By explicitly incorporating PSCs, SST, and a full suite of bio-optical properties, the OCMF inversion model accounts for these factors. In particular, the SST-dependent PSC model increases the contribution of microplankton at low SST, improving representation in regions like the Southern Ocean.

4.4 Model implications and future directions

Ocean-colour research has been advancing beyond a sole focus on Chl-a, increasingly embracing phytoplankton community structure, its dynamics, and interactions with other components of the marine ecosystem. Many recent studies have emphasised the importance of retrieving phytoplankton community structure and IOPs to better characterise biogeochemical processes and ecosystem functions (Nair et al., 2008; IOCCG, 2014; Bracher et al., 2017; Mouw et al., 2017; Cetinić et al., 2024). The OCMF has been developed to further this goal, by simultaneously retrieving phytoplankton size structure, absorption coefficients, and backscattering properties from satellite remote sensing, expanding its applications beyond Chl-a estimation. For example, phytoplankton size affects nutrient uptake, light absorption, sinking rates, and interactions with grazers (Finkel et al., 2009). By incorporating phytoplankton size structure, the model provides insights into community composition, which is important for understanding carbon cycling and energy flow in marine ecosystems (Guidi et al., 2009; Atkinson et al., 2024). A validation of the retrieved PSCs is provided in the Supplementary Section S4.2.4, demonstrating the model's simultaneous inversion capability and showing that the satellite-derived PSCs are consistent with *in-situ* measurements. Meanwhile, understanding IOP variability facilitates in classifying pigment and phytoplankton community composition (Chase et al., 2013; Sun et al., 2022), assessing carbon pools (Evers-King et al., 2017; Fox et al., 2022; Li M. et al., 2024), and improving ecosystem models (Ciavatta et al., 2014; Dutkiewicz et al., 2015). These advancements highlight the value of multi-variable satellite retrievals. Unlike traditional empirical algorithms, the OCMF is also able to account for some level of regional variability in phytoplankton community composition, which has been shown to affect optical properties and ocean colour (Bracher and Tilzer, 2001; Mouw et al., 2012; Barrón et al., 2014). Moreover, the OCMF allows uncertainty propagation from input R_{rs} (e.g., OC-CCI products) to retrieved variables, such as Chl-a, using a Monte Carlo approach with perturbed inputs (see Supplementary Section S4.3). This provides not only concentration estimates but also uncertainties, which are important for climate studies and ecosystem models (Jackson et al., 2017). Despite these advantages, some limitations remain. For example, lower accuracies are observed in specific areas (Section 4.1; Supplementary Section S4.1), likely due to regional optical properties of phytoplankton assemblages and non-algal components not being captured by the model. In addition, the OCMF relies on Chl-a specific absorption and backscattering coefficients derived from previous parameterisation. However, these properties can vary with phytoplankton community composition and change with space and time (e.g., Kheireddine et al., 2018; Bellacicco et al., 2019). This limitation is further influenced by the uneven distribution of *in-situ* measurements (Figure 1), with the some regions being more densely sampled (e.g., the Atlantic Ocean), while some regions remaining under-sampled. Future efforts could focus on refining the bio-optical parameterisation and collecting high-quality optical data to improve performance in these regions.

The application of ocean-colour remote sensing in climate studies has been increasing with the availability of datasets that are sufficient in length to detect trends (e.g., Kulk et al., 2020; Thomalla et al., 2023). Satellite-derived Chl-a trends have been widely used to study phytoplankton responses to climate change, with some studies reporting Chl-a declines in warming waters and others showing regional increases (Antoine et al., 2005; Martinez et al., 2009; Vantrepotte and Mélin, 2011; Gregg and Rousseaux, 2014). Beyond global trends, spatial-temporal changes in phytoplankton dynamics under climate forcing, such as shifts in distribution, bloom timing and intensity, and the structure of productivity zones, have also been investigated (Polovina et al., 2008; Salgado-Hernanz et al., 2019; Turner et al., 2024; Peng et al., 2025). However, differences in dataset length, sensor calibration, and algorithm selection have led to both consistent and contradictory trends across studies (Gregg et al., 2017; Hammond et al., 2017), highlighting the need to re-evaluate long-term changes using consistent models and harmonised datasets (Dierssen, 2010). While most satellite-based climate studies focus solely on Chl-a, a few have investigated shifts in phytoplankton size structure (Montes-Hugo et al., 2009; Polovina and Woodworth, 2012; Lamont et al., 2019; Sun et al., 2019), which can respond differently to environmental and climate-driven changes compared to total Chl-a (Mouw et al., 2019). Accounting for size-fractionated information is therefore important for understanding shifts in ecological function and biogeochemical cycling (Rousseaux and Gregg, 2015). In this context, incorporating SST as an independent variable alongside ocean-colour data is particularly valuable for long-term analyses, as it provides complementary environmental information linked to phytoplankton community structure and helps capture their climate-driven shifts (Ward, 2015; Sun et al., 2023). Furthermore, the complexity of the ocean environment cannot be adequately captured by a single index such as Chl-a. Although widely used, Chl-a may not always reflect phytoplankton carbon biomass due to physiological variability, such as photoacclimation (Siegel et al., 2013; Leonelli et al., 2022). Multi-variable approaches that account for IOPs, including contributions from NAP and CDOM, are necessary for a more comprehensive understanding. Future work will focus on applying OCMF to long-term climate datasets (e.g., OC-CCI) to track changes in Chl-a, phytoplankton size structure, and optical properties over time, providing deeper insights into how phytoplankton respond to global change.

5 Summary

To address the ambiguity in interpreting ocean-colour data, an OCMF was developed, designed to be suitable for constructing long-term records of Chl-a concentration (Sun et al., 2023; Sun et al., 2025). The OCMF explicitly incorporates phytoplankton size structure and IOPs, along with their temperature-dependent

variability, ensuring both biological and optical interpretation. In this third paper of the series, we present an inversion of the OCMF, which retrieves Chl-a and two wavelength-independent parameters (Φ_{dg} and α_d) accounting for deviations in contributions of non-algal substances from standard global conditions. These parameters are retrieved directly from R_{rs} and SST, with information on phytoplankton size structure and optical properties derived simultaneously.

Using a large global dataset of *in-situ* Chl-a and IOPs collected from the surface ocean (≤20 m depth), we conducted a comprehensive validation of the inversion model. Chl-a retrievals were compared across multiple satellite and synthetic datasets, showing consistency with standard products while achieving more stable retrievals, with slopes closer to one across a wide range of Chl-a concentrations, regions, water types, and time periods. This indicates that the OCMF can represent Chl-a variability well, which is particularly important for climate trend analyses. In addition, the model demonstrated good performance for all IOPs, making it suitable for broader ecological and biogeochemical applications. The sensitivity of the OCMF to environmental variability supports its use in the detection of change in phytoplankton community composition. With sound performance and a strong foundation in ecological principles and optical theory, the OCMF provides a valuable tool for understanding long-term changes in phytoplankton in the surface ocean. Its compatibility with hyperspectral observations and neural-network implementation also offer potential for applications in hyperspectral satellite missions and biogeochemical model data assimilation. Future studies will focus on applying the model to long-term satellite datasets to investigate how phytoplankton biomass and community structure evolve under climate change.

Data availability statement

The original contributions presented in the study are included in the article/Supplementary Material, further inquiries can be directed to the corresponding author.

Author contributions

XS: Investigation, Data curation, Writing – review and editing, Software, Visualization, Writing – original draft, Validation, Methodology, Formal Analysis. RoB: Writing – review and editing, Investigation, Supervision, Conceptualization, Methodology, Funding acquisition, Project administration. SS: Investigation, Writing – review and editing. GD: Investigation, Writing – review and editing. DA: Writing – review and editing, Investigation. RaB: Investigation, Writing – review and editing. AB: Writing – review and editing, Investigation. MK: Investigation, Writing – review and editing. ML: Writing – review and editing, Investigation. JP: Investigation, Writing – review and editing. DR: Investigation, Writing – review and editing. FS: Investigation, Writing – review and editing. GT: Writing – review and editing, Investigation. VV: Writing – review and editing, Investigation. YZ: Writing – review and editing, Investigation, Software.

Funding

The author(s) declared that financial support was received for this work and/or its publication. The UKRI Future Leader Fellowship (MR/V022792/1) is the principal source of funding for this work. Additional supports for this work are provided by the United Kingdom National Centre for Earth Observation (NCEO), the Simons Foundation Project Collaboration on Computational Biogeochemical Modeling of Marine Ecosystems (CBIOMES, 549947, Shubha Sathyendranath), and the Royal Society International Exchanges 2021 Cost Share (NSFC) grant (IEC NSFC 211058). The Atlantic Meridional Transect is funded by the UK Natural Environment Research Council through its National Capability Long-term Single Centre Science Programme, Atlantic Climate and Environment Strategic Science - AtlantiS (grant number NE/Y005589/1). This study contributes to the international IMBeR project and is contribution number 426 of the AMT programme. Astrid Bracher was partly funded by the Deutsche Forschungsgemeinschaft (DFG, German Research Foundation)–Projektnummer268020496–TRR 172, within the Transregional Collaborative ResearchCenter "ArctiC Amplification: Climate Relevant Atmospheric and SurfaCe Processes, and Feedback Mechanisms (AC)3" in subproject C03. AWI *in-situ* data were acquired within the framework of the Helmholtz-Infrastructure Initiative FRAM and funding of the Helmholtz-Young-Investigator Group Phytooptics (VH-NG-300). Jaime Pitarch acknowledges partial funding by the European Union—Next Generation EU, Mission 4 "Education and Research"—Component 2: "From research to business"—Investment 3.1: "Fund for the realization of an integrated system of research and innovation infrastructures"-Project IR0000032—ITINERIS—Italian Integrated Environmental Research Infrastructures System—CUPB53C22002150006. Dionysios E. Raitsos acknowledges the European Union HORIZON EUROPE program (ACTNOW, no. 101060072). Fang Shen is funded by the National Natural Science Foundation of China (42530110).

Acknowledgements

The contributors who released *in-situ* data to the public domains, such as the AODN, BCODMO, BODC, BOUSSOLE, DataONE, EDI Data Portal, Government of Canada, NASA SeaBASS, NASA NOMAD, PANGAEA, Rothera Research Station, TARA Ocean, and Western Channel Observatory, are greatly acknowledged. Sincere appreciation is extended to all scientists and crew who worked on the *in-situ* data collection. We are grateful to ESA for providing OC-CCI and Sentinel- 3 OLCI data, NASA for MODIS ocean-colour products, ACRI-ST and Copernicus for the GlobColour dataset, and NOAA for OISST data. This work was supported by the use of NERC JASMIN data analysis facility and the University of Exeter's High-Performance Computing (HPC) facility.

Conflict of interest

The author(s) declared that this work was conducted in the absence of any commercial or financial relationships that could be construed as a potential conflict of interest.

The authors SS, AB declared that they were an editorial board member of Frontiers at the time of submission. This had no impact on the peer review process and the final decision.

Generative AI statement

The author(s) declared that generative AI was not used in the creation of this manuscript.

Any alternative text (alt text) provided alongside figures in this article has been generated by Frontiers with the support of artificial intelligence and reasonable efforts have been made to ensure accuracy, including review by the authors wherever possible. If you identify any issues, please contact us.

Publisher's note

Supplementary material

The Supplementary Material for this article can be found online at: https://www.frontiersin.org/articles/10.3389/frsen.2025.1692306/full#supplementary-material

References

Alvain, S., Loisel, H., and Dessailly, D. (2012). Theoretical analysis of ocean color radiances anomalies and implications for phytoplankton groups detection in case 1 waters. *Opt. Express* 20, 1070–1083. doi:10.1364/OE.20.001070

Álvarez, E., Cossarini, G., Teruzzi, A., Bruggeman, J., Bolding, K., Ciavatta, S., et al. (2023). Chromophoric dissolved organic matter dynamics revealed through the optimization of an optical–biogeochemical model in the northwestern Mediterranean Sea. *Biogeosciences* 20, 4591–4624. doi:10.5194/bg-20-4591-2023

Antoine, D., Morel, A., Gordon, H. R., Banzon, V. F., and Evans, R. H. (2005). Bridging ocean color observations of the 1980s and 2000s in search of long-term trends. *J. Geophys. Res. Oceans* 110. doi:10.1029/2004jc002620

Antoine, D., d'Ortenzio, F., Hooker, S. B., Bécu, G., Gentili, B., Tailliez, D., et al. (2008). Assessment of uncertainty in the ocean reflectance determined by three satellite ocean color sensors (MERIS, SeaWiFS and MODIS-A) at an offshore site in the Mediterranean Sea (BOUSSOLE project). *J. Geophys. Res. Oceans* 113. doi:10.1029/2007jc004472

Antoine, D., Siegel, D. A., Kostadinov, T., Maritorena, S., Nelson, N. B., Gentili, B., et al. (2011). Variability in optical particle backscattering in contrasting bio-optical oceanic regimes. *Limnol. Oceanogr.* 56, 955–973. doi:10.4319/lo.2011.56.3.0955

Arrigo, K. R., Dijken, G. L. van, Alderkamp, A., Erickson, Z. K., Lewis, K. M., Lowry, K. E., et al. (2017). Early spring phytoplankton dynamics in the Western antarctic peninsula. *J. Geophys. Res. Oceans* 122, 9350–9369. doi:10.1002/2017jc013281

Atkinson, A., Rossberg, A. G., Gaedke, U., Sprules, G., Heneghan, R. F., Batziakas, S., et al. (2024). Steeper size spectra with decreasing phytoplankton biomass indicate strong trophic amplification and future fish declines. *Nat. Commun.* 15, 381. doi:10.1038/s41467-023-44406-5

Babin, M., Arrigo, K., Bélanger, S., and Forget, M.-H. (2015). Ocean colour remote sensing in polar seas, *IOCCG report series* No. 16 (Dartmouth, Canada: International Ocean Colour Coordinating Group).

Balch, W. M., Drapeau, D. T., Bowler, B. C., Lyczkowski, E. R., Lubelczyk, L. C., Painter, S. C., et al. (2014). Surface biological, chemical, and optical properties of the patagonian shelf coccolithophore bloom, the brightest waters of the great calcite belt. *Limnol. Oceanogr.* 59, 1715–1732. doi:10.4319/lo.2014.59.5.1715

Barrón, R. K., Siegel, D. A., and Guillocheau, N. (2014). Evaluating the importance of phytoplankton community structure to the optical properties of the Santa Barbara channel, California. *Limnol. Oceanogr.* 59, 927–946. doi:10.4319/lo.2014.59.3.0927

Behrenfeld, M. J., O'Malley, R. T., Siegel, D. A., McClain, C. R., Sarmiento, J. L., Feldman, G. C., et al. (2006). Climate-driven trends in contemporary ocean productivity. *Nature* 444, 752–755. doi:10.1038/nature05317

Behrenfeld, M. J., O'Malley, R. T., Boss, E. S., Westberry, T. K., Graff, J. R., Halsey, K. H., et al. (2015). Revaluating ocean warming impacts on global phytoplankton. *Nat. Clim. Change* 6, 323–330. doi:10.1038/nclimate2838

Bellacicco, M., Volpe, G., Colella, S., Pitarch, J., and Santoleri, R. (2016). Influence of photoacclimation on the phytoplankton seasonal cycle in the Mediterranean Sea as seen by satellite. *Remote Sens. Environ.* 184, 595–604. doi:10.1016/j.rse.2016.08.004

Bellacicco, M., Cornec, M., Organelli, E., Brewin, R. J. W., Neukermans, G., Volpe, G., et al. (2019). Global variability of optical backscattering by non-algal particles from a biogeochemical-argo data set. *Geophys. Res. Lett.* 46, 9767–9776. doi:10.1029/2019gl084078

Biggs, T. E. G., Alvarez-Fernandez, S., Evans, C., Mojica, K. D. A., Rozema, P. D., Venables, H. J., et al. (2019). Antarctic phytoplankton community composition and size structure: importance of ice type and temperature as regulatory factors. *Polar Biol.* 42, 1997–2015. doi:10.1007/s00300-019-02576-3

Bindoff, N. L., Cheung, W. W. L., Kairo, J. G., Arístegui, J., Guinder, V. A., Hallberg, R., et al. (2019). "Changing ocean, marine ecosystems, and dependent communities," in *IPCC special report on the ocean and cryosphere in a changing climate*. Editors H.-O. Pörtner, D. C. Roberts, V. Masson-Delmotte, P. Zhai, M. Tignor, E. Poloczanska, et al. (Cambridge, UK and New York, NY, USA: Cambridge University Press), 447–587.

Bisson, K. M., Boss, E., Werdell, P. J., Ibrahim, A., Frouin, R., and Behrenfeld, M. J. (2021). Seasonal bias in global ocean color observations. *Appl. Opt.* 60, 6978–6988. doi:10.1364/AO.426137

Blondeau-Patissier, D., Gower, J. F. R., Dekker, A. G., Phinn, S. R., and Brando, V. E. (2014). A review of ocean color remote sensing methods and statistical techniques for the detection, mapping and analysis of phytoplankton blooms in coastal and open oceans. *Prog. Oceanogr.* 123, 123–144. doi:10.1016/j.pocean.2013.12.008

Boyce, D. G., Lewis, M. R., and Worm, B. (2010). Global phytoplankton decline over the past century. *Nature* 466, 591–596. doi:10.1038/nature09268

Boyer Montégut, C. de, Madec, G., Fischer, A. S., Lazar, A., and Iudicone, D. (2004). Mixed layer depth over the global ocean: an examination of profile data and a profile-based climatology. *J. Geophys. Res.* 109. doi:10.1029/2004jc002378

Bracher, A., and Tilzer, M. (2001). Underwater light field and phytoplankton absorbance in different surface water masses of the Atlantic sector of the Southern Ocean. *Polar Biol.* 24, 687–696. doi:10.1007/s003000100269

Bracher, A., Bouman, H. A., Brewin, R. J. W., Bricaud, A., Brotas, V., Ciotti, A. M., et al. (2017). Obtaining phytoplankton diversity from ocean color: a scientific roadmap for future development. *Front. Mar. Sci.* 4. doi:10.3389/fmars.2017.00055

Bracher, A., Xi, H., Dinter, T., Mangin, A., Strass, V., Appen, W.-J. von, et al. (2020). High resolution water column phytoplankton composition across the Atlantic Ocean from ship-towed vertical undulating radiometry. *Front. Mar. Sci.* 7, 235. doi:10.3389/fmars.2020.00235

Brewin, R. J. W., Raitsos, D. E., Dall'Olmo, G., Zarokanellos, N., Jackson, T., Racault, M.-F., et al. (2015a). Regional ocean-colour chlorophyll algorithms for the Red Sea. *Remote Sens. Environ.* 165, 64–85. doi:10.1016/j.rse.2015.04.024

Brewin, R. J. W., Sathyendranath, S., Müller, D., Brockmann, C., Deschamps, P.-Y., Devred, E., et al. (2015b). The ocean colour climate change initiative: III. A round-robin comparison on in-water bio-optical algorithms. *Remote Sens. Environ.* 162, 271–294. doi:10.1016/j.rse.2013.09.016

Brewin, R. J. W., Ciavatta, S., Sathyendranath, S., Jackson, T., Tilstone, G., Curran, K., et al. (2017). Uncertainty in ocean-color estimates of chlorophyll for phytoplankton groups. *Front. Mar. Sci.* 4. doi:10.3389/fmars.2017.00104

Brewin, R. J. W., Ciavatta, S., Sathyendranath, S., Skákala, J., Bruggeman, J., Ford, D., et al. (2019). The influence of temperature and community structure on light absorption by phytoplankton in the north Atlantic. *Sensors* 19, 4182. doi:10.3390/s19194182

Bricaud, A., Bosc, E., and Antoine, D. (2002). Algal biomass and sea surface temperature in the Mediterranean Basin. *Remote Sens. Environ.* 81, 163–178. doi:10.1016/s0034-4257(01)00335-2

Brown, C. A., Huot, Y., Werdell, P. J., Gentili, B., and Claustre, H. (2008). The origin and global distribution of second order variability in satellite ocean color and its potential applications to algorithm development. *Remote Sens. Environ.* 112, 4186–4203. doi:10.1016/j.rse.2008.06.008

Bulgarelli, B., and Zibordi, G. (2018). On the detectability of adjacency effects in ocean color remote sensing of mid-latitude coastal environments by SeaWiFS, MODIS-A, MERIS, OLCI, OLI and MSI. *Remote Sens. Environ.* 209, 423–438. doi:10.1016/j.rse.2017.12.021

Campbell, J. W. (1995). The lognormal distribution as a model for bio-optical variability in the sea. *J. Geophys. Res. Oceans* 100, 13237–13254. doi:10.1029/95jc00458

Cetinić, I., Rousseaux, C. S., Carroll, I. T., Chase, A. P., Kramer, S. J., Werdell, P. J., et al. (2024). Phytoplankton composition from sPACE: requirements, opportunities, and challenges. *Remote Sens. Environ.* 302, 113964. doi:10.1016/j.rse.2023.113964

Chase, A., Boss, E., Zaneveld, R., Bricaud, A., Claustre, H., Ras, J., et al. (2013). Decomposition of *in situ* particulate absorption spectra. *Methods Oceanogr.* 7, 110–124. doi:10.1016/j.mio.2014.02.002

Ciavatta, S., Torres, R., Martinez-Vicente, V., Smyth, T., Dall'Olmo, G., Polimene, L., et al. (2014). Assimilation of remotely-sensed optical properties to improve marine biogeochemistry modelling. *Prog. Oceanogr.* 127, 74–95. doi:10.1016/j.pocean.2014.06.002

Ciavatta, S., Brewin, R. J. W., Skákala, J., Polimene, L., Mora, L. de, Artioli, Y., et al. (2018). Assimilation of ocean-color plankton functional types to improve marine ecosystem simulations. *J. Geophys. Res. Oceans* 123, 834–854. doi:10.1002/2017jc013490

Ciavatta, S., Kay, S., Brewin, R. J. W., Cox, R., Di Cicco, A., Nencioli, F., et al. (2019). Ecoregions in the Mediterranean Sea through the reanalysis of Phytoplankton functional types and carbon fluxes. *J. Geophys. Res. Oceans* 124, 6737–6759. doi:10.1029/2019jc015128

Defoin-Platel, M., and Chami, M. (2007). How ambiguous is the inverse problem of ocean color in coastal waters? *J. Geophys. Res.* 112. doi:10.1029/2006jc003847

Demidov, A. B., Gagarin, V. I., and Grigoriev, A. V. (2010). Seasonal variability of the surface chlorophyll "a" in the Drake Passage. *Oceanology* 50, 327–341. doi:10.1134/s0001437010030045

Dierssen, H. M. (2010). Perspectives on empirical approaches for ocean color remote sensing of chlorophyll in a changing climate, *Proc. Natl. Acad. Sci. U. S. A.*, 107: 17073–17078. doi:10.1073/pnas.0913800107

Dierssen, H. M., and Smith, R. C. (2000). Bio-optical properties and remote sensing ocean color algorithms for Antarctic Peninsula waters. *J. Geophys. Res. Oceans* 105, 26301–26312. doi:10.1029/1999jc000296

Dierssen, H. M., Gierach, M., Guild, L. S., Mannino, A., Salisbury, J., Schollaert Uz, S., et al. (2023). Synergies between NASA's hyperspectral aquatic missions PACE, GLIMR, and SBG: opportunities for new science and applications. *J. Geophys. Res. Biogeosciences* 128, e2023JG007574. doi:10.1029/2023jg007574

Dogliotti, A. I., Schloss, I. R., Almandoz, G. O., and Gagliardini, D. A. (2008). Evaluation of SeaWiFS and MODIS chlorophyll-a products in the Argentinean Patagonian Continental Shelf (38° S–55° S). *Int. J. Remote Sens.* 30, 251–273. doi:10.1080/01431160802311133

Dutkiewicz, S., Hickman, A. E., Jahn, O., Gregg, W. W., Mouw, C. B., and Follows, M. J. (2015). Capturing optically important constituents and properties in a marine biogeochemical and ecosystem model. *Biogeosciences* 12, 4447–4481. doi:10.5194/bg-12-4447-2015

El Hourany, R., Abboud-Abi Saab, M., Faour, G., Mejia, C., Crépon, M., and Thiria, S. (2019). Phytoplankton diversity in the Mediterranean Sea from satellite data using self-organizing maps. *J. Geophys. Res. Oceans* 124, 5827–5843. doi:10.1029/2019jc015131

European Union-Copernicus Marine Service (2022). Global ocean colour (Copernicus-GlobColour), bio-geo-chemical, L3 (daily) from satellite observations (1997-ongoing). doi:10.48670/moi-00280

Evers-King, H., Martinez-Vicente, V., Brewin, R. J. W., Dall'Olmo, G., Hickman, A. E., Jackson, T., et al. (2017). Validation and intercomparison of ocean color algorithms for estimating particulate organic carbon in the oceans. *Front. Mar. Sci.* 4, 251. doi:10.3389/fmars.2017.00251

Ferreira, A., Ciotti, Á. M., and Garcia, C. A. E. (2018). Bio-optical characterization of the northern Antarctic Peninsula waters: absorption budget and insights on particulate backscattering. *Deep Sea Res. Part II Top. Stud. Oceanogr.* 149, 138–149. doi:10.1016/j.dsr2.2017.09.007

Ferreira, A., Mendes, C. R. B., Costa, R. R., Brotas, V., Tavano, V. M., Guerreiro, C. V., et al. (2024). Climate change is associated with higher phytoplankton biomass and longer blooms in the West Antarctic Peninsula. *Nat. Commun.* 15, 6536. doi:10.1038/s41467-024-50381-2

Field, C. B., Behrenfeld, M. J., Randerson, J. T., and Falkowski, P. (1998). Primary production of the biosphere: integrating terrestrial and Oceanic components. *Science* 281, 237–240. doi:10.1126/science.281.5374.237

Finkel, Z. V., Beardall, J., Flynn, K. J., Quigg, A., Rees, T. A. V., and Raven, J. A. (2009). Phytoplankton in a changing world: cell size and elemental stoichiometry. *J. Plankton Res.* 32, 119–137. doi:10.1093/plankt/fbp098

Fox, J., Kramer, S. J., Graff, J. R., Behrenfeld, M. J., Boss, E., Tilstone, G., et al. (2022). An absorption-based approach to improved estimates of phytoplankton biomass and net primary production. *Limnol. Oceanogr. Lett.* 7, 419–426. doi:10.1002/lol2.10275

Garcia, V. M. T., Garcia, C. A. E., Mata, M. M., Pollery, R. C., Piola, A. R., Signorini, S. R., et al. (2008). Environmental factors controlling the phytoplankton blooms at the Patagonia shelf-break in spring. *Deep Sea Res. Part I Oceanogr. Res. Pap.* 55, 1150–1166. doi:10.1016/j.dsr.2008.04.011

Garnesson, P., Mangin, A., Fanton d'Andon, O., Demaria, J., and Bretagnon, M. (2019). The CMEMS GlobColour chlorophyll a product based on satellite observation: multi-sensor merging and flagging strategies. *Ocean Sci.* 15, 819–830. doi:10.5194/os-15-819-2019

Gregg, W. W., and Rousseaux, C. S. (2014). Decadal trends in global pelagic ocean chlorophyll: a new assessment integrating multiple satellites, *in situ* data, and models. *J. Geophys. Res. Oceans* 119, 5921–5933. doi:10.1002/2014JC010158

Gregg, W. W., Rousseaux, C. S., and Franz, B. A. (2017). Global trends in ocean phytoplankton: a new assessment using revised ocean colour data. *Remote Sens. Lett.* 8, 1102–1111. doi:10.1080/2150704X.2017.1354263

Guidi, L., Stemmann, L., Jackson, G. A., Ibanez, F., Claustre, H., Legendre, L., et al. (2009). Effects of phytoplankton community on production, size, and export of large aggregates: a world-ocean analysis. *Limnol. Oceanogr.* 54, 1951–1963. doi:10.4319/lo.2009.54.6.1951

Guinder, V. A., Ferronato, C., Dogliotti, A. I., Segura, V., and Lutz, V. (2024). "The phytoplankton of the Patagonian shelf-break front," in *The patagonian shelfbreak front* (Switzerland: Springer Nature), 49–72.

Hammond, M. L., Beaulieu, C., Sahu, S. K., and Henson, S. A. (2017). Assessing trends and uncertainties in satellite-era ocean chlorophyll using space-time modeling. *Glob. Biogeochem. Cycles* 31, 1103–1117. doi:10.1002/2016gb005600

Hammond, M. L., Beaulieu, C., Henson, S. A., and Sahu, S. K. (2020). Regional surface chlorophyll trends and uncertainties in the global ocean. *Sci. Rep.* 10, 15273. doi:10.1038/s41598-020-72073-9

Hammoud, M. A. E. R., Papagiannopoulos, N., Krokos, G., Brewin, R. J. W., Raitsos, D. E., Knio, O., et al. (2025). On the potential of Bayesian neural networks for estimating Chlorophyll-a concentration from satellite data. *Remote Sens.* 17, 1826. doi:10.3390/rs17111826

Hayward, A., Pinkerton, M. H., Wright, S. W., Gutiérrez-Rodriguez, A., and Law, C. S. (2024). Twenty-six years of phytoplankton pigments reveal a circumpolar class divide around the Southern Ocean. *Commun. Earth and Environ.* 5, 92. doi:10.1038/s43247-024-01261-6

Henson, S. A., Sarmiento, J. L., Dunne, J. P., Bopp, L., Lima, I., Doney, S. C., et al. (2010). Detection of anthropogenic climate change in satellite records of ocean chlorophyll and productivity. *Biogeosciences* 7, 621–640. doi:10.5194/bg-7-621-2010

HOT-DOGS (2024). *Hawaii ocean Time-series HOT-DOGS application*. University of Hawai'i at Mānoa. National Science Foundation. Award #2241005. Available online at: https://hahana.soest.hawaii.edu/hot/hot-dogs/

Hu, C., Feng, L., Lee, Z., Davis, C. O., Mannino, A., McClain, C. R., et al. (2012). Dynamic range and sensitivity requirements of satellite ocean color sensors: learning from the past. *Appl. Opt.* 51, 6045–6062. doi:10.1364/AO.51.006045

Hu, C., Feng, L., Lee, Z., Franz, B. A., Bailey, S. W., Werdell, P. J., et al. (2019). Improving satellite global chlorophyll a data products through Algorithm refinement and data recovery. *J. Geophys. Res. Oceans* 124, 1524–1543. doi:10.1029/2019jc014941

Hutchins, D. A., and Tagliabue, A. (2024). Feedbacks between phytoplankton and nutrient cycles in a warming ocean. *Nat. Geosci.* 17, 495–502. doi:10.1038/s41561-024-01454-w

IOCCG (2014). "*Phytoplankton functional types from space*," Reports International Ocean-Colour Coordinating Group. Canada: Dartmouth, Nova Scotia. Available online at: https://ioccg.org/wp-content/uploads/2018/09/ioccg_report_15_2014.pdf.

Jackson, T., Sathyendranath, S., and Mélin, F. (2017). An improved optical classification scheme for the ocean colour essential climate variable and its applications. *Remote Sens. Environ.* 203, 152–161. doi:10.1016/j.rse.2017.03.036

Johnson, R., Strutton, P. G., Wright, S. W., McMinn, A., and Meiners, K. M. (2013). Three improved satellite chlorophyll algorithms for the Southern OceanS. *J. Geophys. Res. Oceans* 118, 3694–3703. doi:10.1002/jgrc.20270

Johnson, R. J., Bates, N., Lethaby, P. J., Medley, C., and Smith, D. (2023). HPLC pigment concentrations from the Bermuda Atlantic Time-series study (BATS) site from 1988-2022.

Jordan, T., Dall'Olmo, G., Tilstone, G., Brewin, R., Nencioli, F., Ruth, A., et al. (2024a). Surface inherent optical properties and phytoplankton pigment concentrations from the Atlantic meridional transect (2009 - 2019): NetCDF format.

Jordan, T. M., Dall'Olmo, G., Tilstone, G., Brewin, R. J. W., Nencioli, F., Airs, R., et al. (2024b). A compilation of surface inherent optical properties and phytoplankton pigment concentrations from the Atlantic meridional transect. *Earth Syst. Sci. Data* 17, 493–516. doi:10.5194/essd-17-493-2025

Kavanaugh, M., Bell, T., Catlett, D., Cimino, M., Doney, S., Klajbor, W., et al. (2021). Satellite remote sensing and the marine biodiversity observation network: current science and future steps. *Oceanography* 34. doi:10.5670/oceanog.2021.215

Kheireddine, M., and Antoine, D. (2014). Diel variability of the beam attenuation and backscattering coefficients in the northwestern Mediterranean Sea (BOUSSOLE site). *J. Geophys. Res. Oceans* 119, 5465–5482. doi:10.1002/2014jc010007

Kheireddine, M., Ouhssain, M., Organelli, E., Bricaud, A., and Jones, B. H. (2018). Light absorption by suspended particles in the Red Sea: effect of Phytoplankton community size structure and pigment composition. *J. Geophys. Res. Oceans* 123, 902–921. doi:10.1002/2017jc013279

Kingma, D. P., and Ba, J. (2014). Adam: a method for stochastic optimization. *arXiv: 1412.6980*. doi:10.48550/arXiv.1412.6980

Kournopoulou, A., Kikaki, K., Varkitzi, I., Psarra, S., Assimakopoulou, G., Karantzalos, K., et al. (2024). Atlas of phytoplankton phenology indices in selected Eastern Mediterranean marine ecosystems. *Sci. Rep.* 14, 9975. doi:10.1038/s41598-024-60792-2

Kulk, G., Platt, T., Dingle, J., Jackson, T., Jönsson, B., Bouman, H., et al. (2020). Primary production, an index of climate change in the ocean: Satellite-based estimates over two decades. *Remote Sens.* 12, 826. doi:10.3390/rs12050826

Lamont, T., Barlow, R. G., and Brewin, R. J. W. (2019). Long-term trends in Phytoplankton chlorophyll a and size structure in the Benguela upwelling system. *J. Geophys. Res. Oceans* 124, 1170–1195. doi:10.1029/2018jc014334

Lavigne, H., D'Ortenzio, F., Migon, C., Claustre, H., Testor, P., d'Alcalà, M. R., et al. (2013). Enhancing the comprehension of mixed layer depth control on the Mediterranean phytoplankton phenology: mediterranean Phytoplankton Phenology. *J. Geophys. Res. Oceans* 118, 3416–3430. doi:10.1002/jgrc.20251

Lavigne, H., Zande, D. V. der, Ruddick, K., Cardoso Dos Santos, J. F., Gohin, F., Brotas, V., et al. (2021). Quality-control tests for OC4, OC5 and NIR-red satellite chlorophyll-a algorithms applied to coastal waters. *Remote Sens. Environ.* 255, 112237. doi:10.1016/j.rse.2020.112237

Lee, Z., Carder, K. L., and Arnone, R. A. (2002). Deriving inherent optical properties from water color: a multiband quasi-analytical algorithm for optically deep waters. *Appl. Opt.* 41, 5755–5772. doi:10.1364/ao.41.005755

Lee, Z. P., Du, K., Voss, K. J., Zibordi, G., Lubac, B., Arnone, R., et al. (2011). An inherent-optical-property-centered approach to correct the angular effects in water-leaving radiance. *Appl. Opt.* 50, 3155–3167. doi:10.1364/AO.50.003155

Lee, Z., Hu, C., Shang, S., Du, K., Lewis, M., Arnone, R., et al. (2013). Penetration of UV-visible solar radiation in the global oceans: insights from ocean color remote sensing. *J. Geophys. Res. Oceans* 118, 4241–4255. doi:10.1002/jgrc.20308

Lee, Z., Wei, J., Voss, K., Lewis, M., Bricaud, A., and Huot, Y. (2015). Hyperspectral absorption coefficient of "pure" seawater in the range of 350-550 nm inverted from remote sensing reflectance. *Appl. Opt.* 54, 546. doi:10.1364/ao.54.000546

Lee, Z., Shang, S., Zhang, S., Wu, J., Wei, G., and Wu, X. (2020). Impact of temporal variation of chlorophyll-specific absorption on phytoplankton phenology observed from ocean color satellite: a numerical experiment. *J. Geophys. Res. Oceans* 125, e2020JC016382. doi:10.1029/2020jc016382

Leonelli, F. E., Bellacicco, M., Pitarch, J., Organelli, E., Buongiorno Nardelli, B., Toma, V. de, et al. (2022). Ultra-oligotrophic waters expansion in the North Atlantic subtropical gyre revealed by 21 years of satellite observations. *Geophys. Res. Lett.* 49, e2021GL096965. doi:10.1029/2021gl096965

Lewis, K. M., and Arrigo, K. R. (2020). Ocean color algorithms for estimating chlorophyll a, CDOM absorption, and particle backscattering in the Arctic Ocean. *J. Geophys. Res. Oceans* 125, e2019JC015706. doi:10.1029/2019jc015706

Li, X., Yang, Y., Ishizaka, J., and Li, X. (2023). Global estimation of phytoplankton pigment concentrations from satellite data using a deep-learning-based model. *Remote Sens. Environ.* 294, 113628. doi:10.1016/j.rse.2023.113628

Li, J., Matsuoka, A., Pang, X., Massicotte, P., and Babin, M. (2024a). Performance of algorithms for retrieving chlorophyll a concentrations in the Arctic Ocean: impact on primary production estimates. *Remote Sens.* 16, 892. doi:10.3390/rs16050892

Li, M., Shen, F., Organelli, E., Luo, W., Li, R., Sun, X., et al. (2024b). Disentangling particle composition to improve space-based quantification of POC in optically complex estuarine and coastal waters. *IEEE Trans. Geoscience Remote Sens.* 62, 1–15. doi:10.1109/tgrs.2023.3341462

Loisel, H., Vantrepotte, V., Norkvist, K., Mériaux, X., Kheireddine, M., Ras, J., et al. (2011). Characterization of the bio-optical anomaly and diurnal variability of particulate matter, as seen from scattering and backscattering coefficients, in ultra-oligotrophic eddies of the Mediterranean Sea. *Biogeosciences* 8, 3295–3317. doi:10.5194/bg-8-3295-2011

Lomas, M. (2021). Size-fractionated chlorophyll collected from CTD samples in Chukchi Seas during Arctic integrated ecosystem research Program 2019. *Research Workspace*. doi:10.24431/rw1k58m

Longhurst, A., Sathyendranath, S., Platt, T., and Caverhill, C. (1995). An estimate of global primary production in the ocean from satellite radiometer data. *J. Plankton Res.* 17, 1245–1271. doi:10.1093/plankt/17.6.1245

Marañón, E., Cermeño, P., Latasa, M., and Tadonléké, R. D. (2012). Temperature, resources, and phytoplankton size structure in the ocean. *Limnol. Oceanogr.* 57, 1266–1278. doi:10.4319/lo.2012.57.5.1266

Maritorena, S., Siegel, D. A., and Peterson, A. R. (2002). Optimization of a semianalytical ocean color model for global-scale applications. *Appl. Opt.* 41, 2705–2714. doi:10.1364/ao.41.002705

Martinez, E., Antoine, D., D'Ortenzio, F., and Gentili, B. (2009). Climate-driven basin-scale decadal oscillations of Oceanic phytoplankton. *Science* 326, 1253–1256. doi:10.1126/science.1177012

Marty, J.-C., Chiavérini, J., Pizay, M.-D., and Avril, B. (2002). Seasonal and interannual dynamics of nutrients and phytoplankton pigments in the Western Mediterranean Sea at the DYFAMED time-series station (1991–1999). *Deep Sea Res. Part II Top. Stud. Oceanogr.* 49, 1965–1985. doi:10.1016/s0967-0645(02)00022-x

Mayot, N., D'Ortenzio, F., Uitz, J., Gentili, B., Ras, J., Vellucci, V., et al. (2017). Influence of the Phytoplankton community structure on the spring and annual primary production in the Northwestern Mediterranean Sea. *J. Geophys. Res. Oceans* 122, 9918–9936. doi:10.1002/2016jc012668

McClain, C. R. (2009). A decade of satellite ocean color observations. *Annu. Rev. Mar. Sci.* 1, 19–42. doi:10.1146/annurev.marine.010908.163650

Mélin, F., Zibordi, G., and Berthon, J.-F. (2007). Assessment of satellite ocean color products at a coastal site. *Remote Sens. Environ.* 110, 192–215. doi:10.1016/j.rse.2007.02.026

Montes-Hugo, M., Doney, S. C., Ducklow, H. W., Fraser, W., Martinson, D., Stammerjohn, S. E., et al. (2009). Recent changes in phytoplankton communities associated with rapid regional climate change along the Western antarctic peninsula. *Science* 323, 1470–1473. doi:10.1126/science.1164533

Morel, A., and Gentili, B. (2009). A simple band ratio technique to quantify the colored dissolved and detrital organic material from ocean color remotely sensed data. *Remote Sens. Environ.* 113, 998–1011. doi:10.1016/j.rse.2009.01.008

Morel, A., and Maritorena, S. (2001). Bio-optical properties of oceanic waters: a reappraisal. *J. Geophys. Res. Oceans* 106, 7163–7180. doi:10.1029/2000jc000319

Morel, A., and Prieur, L. (1977). Analysis of variations in ocean color1. *Limnol. Oceanogr.* 22, 709–722. doi:10.4319/lo.1977.22.4.0709

Morel, A., Huot, Y., Gentili, B., Werdell, P. J., Hooker, S. B., and Franz, B. A. (2007). Examining the consistency of products derived from various ocean color sensors in open ocean (case 1) waters in the perspective of a multi-sensor approach. *Remote Sens. Environ.* 111, 69–88. doi:10.1016/j.rse.2007.03.012

Mouw, C. B., Yoder, J. A., and Doney, S. C. (2012). Impact of phytoplankton community size on a linked global ocean optical and ecosystem model. *J. Mar. Syst.* 89, 61–75. doi:10.1016/j.jmarsys.2011.08.002

Mouw, C. B., Hardman-Mountford, N. J., Alvain, S., Bracher, A., Brewin, R. J. W., Bricaud, A., et al. (2017). A consumer's guide to satellite remote sensing of multiple phytoplankton groups in the global ocean. *Front. Mar. Sci.* 4. doi:10.3389/fmars.2017.00041

Mouw, C. B., Ciochetto, A. B., and Yoder, J. A. (2019). A satellite assessment of environmental controls of Phytoplankton community size structure. *Glob. Biogeochem. Cycles* 33, 540–558. doi:10.1029/2018gb006118

Nair, V., and Hinton, G. E. (2010). "Rectified linear units improve restricted Boltzmann machines," in *International conference on machine learning*.

Nair, A., Sathyendranath, S., Platt, T., Morales, J., Stuart, V., Forget, M.-H., et al. (2008). Remote sensing of phytoplankton functional types. *Remote Sens. Environ.* 112, 3366–3375. doi:10.1016/j.rse.2008.01.021

Navarro, G., Almaraz, P., Caballero, I., Vázquez, A., and Huertas, I. E. (2017). Reproduction of spatio-temporal patterns of major Mediterranean phytoplankton groups from remote sensing OC-CCI data. *Front. Mar. Sci.* 4, 246. doi:10.3389/fmars.2017.00246

Organelli, E., Bricaud, A., Antoine, D., and Matsuoka, A. (2014). Seasonal dynamics of light absorption by chromophoric dissolved organic matter (CDOM) in the NW Mediterranean Sea (BOUSSOLE site). *Deep Sea Res. Part I Oceanogr. Res. Pap.* 91, 72–85. doi:10.1016/j.dsr.2014.05.003

Organelli, E., Bricaud, A., Gentili, B., Antoine, D., and Vellucci, V. (2016). Retrieval of colored detrital matter (CDM) light absorption coefficients in the Mediterranean Sea using field and satellite ocean color radiometry: evaluation of bio-optical inversion models. *Remote Sens. Environ.* 186, 297–310. doi:10.1016/j.rse.2016.08.028

Ortega-Retuerta, E., Siegel, D. A., Nelson, N. B., Duarte, C. M., and Reche, I. (2010). Observations of chromophoric dissolved and detrital organic matter distribution using remote sensing in the Southern Ocean: validation, dynamics and regulation. *J. Mar. Syst.* 82, 295–303. doi:10.1016/j.jmarsys.2010.06.004

O'Reilly, J. E., and Werdell, P. J. (2019). Chlorophyll algorithms for ocean color sensors - OC4, OC5 and OC6. *Remote Sens. Environ.* 229, 32–47. doi:10.1016/j.rse.2019.04.021

Pahlevan, N., Smith, B., Alikas, K., Anstee, J., Barbosa, C., Binding, C., et al. (2022). Simultaneous retrieval of selected optical water quality indicators from Landsat-8, Sentinel-2, and Sentinel-3. *Remote Sens. Environ.* 270, 112860. doi:10.1016/j.rse.2021.112860

Pauthenet, E., Martinez, E., Gorgues, T., Roussillon, J., Drumetz, L., Fablet, R., et al. (2024). Contrasted trends in Chlorophyll-a satellite products. *Geophys. Res. Lett.* 51, e2024GL108916. doi:10.1029/2024gl108916

Peng, S., Yu, X., Lee, Z., Lin, H., Liu, X., Dai, M., et al. (2025). Ocean's largest chlorophyll-rich tongue is extending westward (2002–2022). *Nat. Commun.* 16, 103. doi:10.1038/s41467-024-55650-8

Pitarch, J., and Brando, V. E. (2025). A hyperspectral and multi-angular synthetic dataset for algorithm development in waters of varying trophic levels and optical complexity. *Earth Syst. Sci. Data* 17, 435–460. doi:10.5194/essd-17-435-2025

Platt, T., and Sathyendranath, S. (2008). Ecological indicators for the pelagic zone of the ocean from remote sensing. *Remote Sens. Environ.* 112, 3426–3436. doi:10.1016/j.rse.2007.10.016

Polovina, J. J., and Woodworth, P. A. (2012). Declines in phytoplankton cell size in the subtropical oceans estimated from satellite remotely-sensed temperature and chlorophyll, 1998–2007. *Deep Sea Res. Part II Top. Stud. Oceanogr.* 77–80, 82–88. doi:10.1016/j.dsr2.2012.04.006

Polovina, J. J., Howell, E. A., and Abecassis, M. (2008). Ocean's least productive waters are expanding. *Geophys. Res. Lett.* 35. doi:10.1029/2007gl031745

Pope, R. M., and Fry, E. S. (1997). Absorption spectrum (380–700 nm) of pure water. II. Integrating cavity measurements. *Appl. Opt.* 36, 8710–8723. doi:10.1364/ao.36.008710

Pradhan, H. K., Völker, C., Losa, S. N., Bracher, A., and Nerger, L. (2020). Global assimilation of ocean-color data of Phytoplankton functional types: impact of different data sets. *J. Geophys. Res. Oceans* 125, e2019JC015586. doi:10.1029/2019jc015586

Prechelt, L. (1998). "Early stopping - but when?," in *Neural networks: tricks of the trade* (Berlin Heidelberg: Springer), 55–69.

Robinson, C. M., Huot, Y., Schuback, N., Ryan-Keogh, T. J., Thomalla, S. J., and Antoine, D. (2021). High latitude Southern Ocean phytoplankton have distinctive bio-optical properties. *Opt. Express* 29, 21084–21112. doi:10.1364/OE.426737

Rousseaux, C. S., and Gregg, W. W. (2015). Recent decadal trends in global phytoplankton composition. *Glob. Biogeochem. Cycles* 29, 1674–1688. doi:10.1002/2015gb005139

Salgado-Hernanz, P. M., Racault, M.-F., Font-Muñoz, J. S., and Basterretxea, G. (2019). Trends in phytoplankton phenology in the Mediterranean Sea based on ocean-colour remote sensing. *Remote Sens. Environ.* 221, 50–64. doi:10.1016/j.rse.2018.10.036

Salyuk, P. A., Glukhovets, D. I., Latushkin, A. A., Kalinina, O. Y., Shtraikhert, E. A., Sapozhnikov, P. V., et al. (2025). Extreme underestimation of satellite-derived chlorophyll-a concentration in the northwestern Weddell Sea during a phytoplankton bloom and its reasons. *J. Mar. Syst.* 252, 104159. doi:10.1016/j.jmarsys.2025.104159

Sathyendranath, S., Cota, G., Stuart, V., Maass, H., and Platt, T. (2001). Remote sensing of phytoplankton pigments: a comparison of empirical and theoretical approaches. *Int. J. Remote Sens.* 22, 249–273. doi:10.1080/014311601449925

Sathyendranath, S., Brewin, R. J. W., Jackson, T., Mélin, F., and Platt, T. (2017). Ocean-colour products for climate-change studies: what are their ideal characteristics? *Remote Sens. Environ.* 203, 125–138. doi:10.1016/j.rse.2017.04.017

Sathyendranath, S., Brewin, R., Brockmann, C., Brotas, V., Calton, B., Chuprin, A., et al. (2019). An ocean-colour time series for use in climate studies: the experience of the ocean-colour climate change initiative (OC-CCI). *Sensors* 19, 4285. doi:10.3390/s19194285

Sathyendranath, S., Jackson, T., Brockmann, C., Brotas, V., Calton, B., Chuprin, A., et al. (2021). ESA ocean colour climate change initiative (Ocean_Colour_cci): version 5.0 data.

Sathyendranath, S., Brewin, R. J. W., Ciavatta, S., Jackson, T., Kulk, G., Jönsson, B., et al. (2023). Ocean biology studied from space. *Surv. Geophys.* 44, 1287–1308. doi:10.1007/s10712-023-09805-9

Sauer, M. J., Roesler, C. S., Werdell, P. J., and Barnard, A. (2012). Under the hood of satellite empirical chlorophyll a algorithms: revealing the dependencies of maximum band ratio algorithms on inherent optical properties. *Opt. Express* 20, 20920–20933. doi:10.1364/OE.20.020920

Schofield, O., Saba, G., Coleman, K., Carvalho, F., Couto, N., Ducklow, H., et al. (2017). Decadal variability in coastal phytoplankton community composition in a changing West Antarctic Peninsula. *Deep Sea Res. Part I Oceanogr. Res. Pap.* 124, 42–54. doi:10.1016/j.dsr.2017.04.014

Shi, C., Hashimoto, M., Shiomi, K., and Nakajima, T. (2021). Development of an Algorithm to retrieve aerosol optical properties over water using an artificial neural network radiative transfer scheme: first result from GOSAT-2/CAI-2. *IEEE Trans. Geoscience Remote Sens.* 59, 9861–9872. doi:10.1109/tgrs.2020.3038892

Sieburth, J. M., Smetacek, V., and Lenz, J. (1978). Pelagic ecosystem structure: heterotrophic compartments of the plankton and their relationship to plankton size fractions 1. *Limnol. Oceanogr.* 23, 1256–1263. doi:10.4319/lo.1978.23.6.1256

Siegel, D. A., Behrenfeld, M. J., Maritorena, S., McClain, C. R., Antoine, D., Bailey, S. W., et al. (2013). Regional to global assessments of phytoplankton dynamics from the SeaWiFS mission. *Remote Sens. Environ.* 135, 77–91. doi:10.1016/j.rse.2013.03.025

Signorini, S. R., Garcia, V. M. T., Piola, A. R., Garcia, C. A. E., Mata, M. M., and McClain, C. R. (2006). Seasonal and interannual variability of calcite in the vicinity of the Patagonian shelf break (38°S–52°S). *Geophys. Res. Lett.* 33. doi:10.1029/2006gl026592

Stock, A., and Subramaniam, A. (2022). Iterative spatial leave-one-out cross-validation and gap-filling based data augmentation for supervised learning applications in marine remote sensing. *GIScience and Remote Sens.* 59, 1281–1300. doi:10.1080/15481603.2022.2107113

Stramski, D., Bricaud, A., and Morel, A. (2001). Modeling the inherent optical properties of the ocean based on the detailed composition of the planktonic community. *Appl. Opt.* 40, 2929–2945. doi:10.1364/ao.40.002929

Sun, X., Shen, F., Brewin, R. J. W., Liu, D., and Tang, R. (2019). Twenty-Year variations in satellite-derived Chlorophyll-a and phytoplankton size in the Bohai Sea and yellow sea. *J. Geophys. Res. Oceans* 124, 8887–8912. doi:10.1029/2019jc015552

Sun, X., Shen, F., Brewin, R. J. W., Li, M., and Zhu, Q. (2022). Light absorption spectra of naturally mixed phytoplankton assemblages for retrieval of phytoplankton group composition in coastal oceans. *Limnol. Oceanogr.* 67, 946–961. doi:10.1002/lno.12047

Sun, X., Brewin, R. J. W., Sathyendranath, S., Dall'Olmo, G., Airs, R., Barlow, R., et al. (2023). Coupling ecological concepts with an ocean-colour model: phytoplankton size structure. *Remote Sens. Environ.* 285, 113415. doi:10.1016/j.rse.2022.113415

Sun, X., Brewin, R. J. W., Sathyendranath, S., Dall'Olmo, G., Antoine, D., Barlow, R., et al. (2025). Coupling ecological concepts with an ocean-colour model: parameterisation and forward modelling. *Remote Sens. Environ.* 316, 114487. doi:10.1016/j.rse.2024.114487

Szeto, M., Werdell, P. J., Moore, T. S., and Campbell, J. W. (2011). Are the world's oceans optically different? *J. Geophys. Res. Oceans* 116. doi:10.1029/2011jc007230

Terhaar, J., Burger, F. A., Vogt, L., Frölicher, T. L., and Stocker, T. F. (2025). Record sea surface temperature jump in 2023–2024 unlikely but not unexpected. *Nature* 639, 942–946. doi:10.1038/s41586-025-08674-z

Thomalla, S. J., Nicholson, S.-A., Ryan-Keogh, T. J., and Smith, M. E. (2023). Widespread changes in Southern Ocean phytoplankton blooms linked to climate drivers. *Nat. Clim. Change* 13, 975–984. doi:10.1038/s41558-023-01768-4

Thomas, M. K., Kremer, C. T., Klausmeier, C. A., and Litchman, E. (2012). A global pattern of thermal adaptation in marine Phytoplankton. *Science* 338, 1085–1088. doi:10.1126/science.1224836

Trimborn, S., Hoppe, C. J. M., Taylor, B. B., Bracher, A., and Hassler, C. (2015). Physiological characteristics of open ocean and coastal phytoplankton communities of Western Antarctic Peninsula and Drake Passage waters. *Deep Sea Res. Part I Oceanogr. Res. Pap.* 98, 115–124. doi:10.1016/j.dsr.2014.12.010

Turner, J. S., Dierssen, H., Schofield, O., Kim, H. H., Stammerjohn, S., Munro, D. R., et al. (2024). Changing phytoplankton phenology in the marginal ice zone west of the Antarctic Peninsula. *Mar. Ecol. Prog. Ser.* 734, 1–21. doi:10.3354/meps14567

Uitz, J., Claustre, H., Morel, A., and Hooker, S. B. (2006). Vertical distribution of phytoplankton communities in open ocean: an assessment based on surface chlorophyll. *J. Geophys. Res.* 111. doi:10.1029/2005jc003207

Uitz, J., Claustre, H., Gentili, B., and Stramski, D. (2010). Phytoplankton class-specific primary production in the world's oceans: seasonal and interannual variability from satellite observations. *Glob. Biogeochem. Cycles* 24. doi:10.1029/2009gb003680

Vantrepotte, V., and Mélin, F. (2011). Inter-annual variations in the SeaWiFS global chlorophyll a concentration (1997–2007). *Deep Sea Res. Part I Oceanogr. Res. Pap.* 58, 429–441. doi:10.1016/j.dsr.2011.02.003

Viljoen, J. J., and Fietz, S. (2021). Surface summer phytoplankton pigment concentrations measured by HPLC during the SANAE-56 cruise in the Atlantic Southern Ocean between December 2016 and February 2017.

Viljoen, J. J., Sun, X., and Brewin, R. J. W. (2024). Climate variability shifts the vertical structure of phytoplankton in the Sargasso Sea. *Nat. Clim. Change* 14, 1292–1298. doi:10.1038/s41558-024-02136-6

Volpe, G., Santoleri, R., Vellucci, V., Ribera d'Alcalà, M., Marullo, S., and D'Ortenzio, F. (2007). The colour of the Mediterranean Sea: global versus regional bio-optical algorithms evaluation and implication for satellite chlorophyll estimates. *Remote Sens. Environ.* 107, 625–638. doi:10.1016/j.rse.2006.10.017

Volpe, G., Nardelli, B. B., Cipollini, P., Santoleri, R., and Robinson, I. S. (2012). Seasonal to interannual phytoplankton response to physical processes in the Mediterranean Sea from satellite observations. *Remote Sens. Environ.* 117, 223–235. doi:10.1016/j.rse.2011.09.020

Ward, B. A. (2015). Temperature-correlated changes in Phytoplankton community structure are restricted to polar waters. *PLOS ONE* 10, e0135581. doi:10.1371/journal.pone.0135581

Wei, J., and Aurin, D. (2020). Python code for calculating the Rrs spectra quality assurance (QA) scores (v2.0).

Wei, J., Lee, Z., and Shang, S. (2016). A system to measure the data quality of spectral remote sensing reflectance of aquatic environments. *J. Geophys. Res. Oceans*. doi:10.1002/2016jc012126

Werdell, P. J., Franz, B. A., Bailey, S. W., Feldman, G. C., Boss, E., Brando, V. E., et al. (2013). Generalized ocean color inversion model for retrieving marine inherent optical properties. *Appl. Opt.* 52, 2019–2037. doi:10.1364/AO.52.002019

Zhang, X., and Hu, L. (2009). Estimating scattering of pure water from density fluctuation of the refractive index. *Opt. Express* 17, 1671–1678. doi:10.1364/oe.17.001671

Zhang, X., Hu, L., and He, M.-X. (2009). Scattering by pure seawater: effect of salinity. *Opt. Express* 17, 5698–5710. doi:10.1364/oe.17.005698

Zhang, X., Hu, L., Xiong, Y., Huot, Y., and Gray, D. (2020). Experimental estimates of optical backscattering associated with submicron particles in clear Oceanic waters. *Geophys. Res. Lett.* 47, e2020GL087100. doi:10.1029/2020gl087100

Zhang, X., Shi, C., Si, Y., Letu, H., Wang, L., Tang, C., et al. (2023a). Remote sensing of aerosols and water-leaving radiance from Chinese FY-3/MERSI based on a simultaneous method. *Remote Sens.* 15, 5650. doi:10.3390/rs15245650

Zhang, Y., Shen, F., Sun, X., and Tan, K. (2023b). Marine big data-driven ensemble learning for estimating global phytoplankton group composition over two decades (1997–2020). *Remote Sens. Environ.* 294, 113596. doi:10.1016/j.rse.2023.113596

Zhang, Y., Shen, F., Li, R., Li, M., Li, Z., Chen, S., et al. (2024). AIGD-PFT: the first AI-driven global daily gap-free 4 km phytoplankton functional type data product from 1998 to 2023. *Earth Syst. Sci. Data* 16, 4793–4816. doi:10.5194/essd-16-4793-2024

Zheng, G., and DiGiacomo, P. M. (2017). Uncertainties and applications of satellite-derived coastal water quality products. *Prog. Oceanogr.* 159, 45–72. doi:10.1016/j.pocean.2017.08.007